LXR-inducible host E3 ligase IDOL targets a human cytomegalovirus reactivation determinant

Luwanika Mlera[1,2], Donna Collins-McMillen[1,2], Sebastian Zeltzer[1,2], Jason C. Buehler[1,2†], Melissa Moy[3†], Kristen Zarrella[1], Katie Caviness[1,2,4§], Louis Cicchini[2,5¶], David J. Tafoya[1,2], and Felicia Goodrum[1,2,3,5*]

[1]Department of Immunobiology, University of Arizona, Tucson, AZ 85721, USA

[2]BIO5 Institute, University of Arizona, Tucson, AZ 85721, USA

[3]Graduate Interdisciplinary Program in Cancer Biology, University of Arizona, Tucson, AZ 85721, USA

[4]Graduate Interdisciplinary Program in Genetics, University of Arizona, Tucson, AZ 85721, USA

[5]Department of Molecular and Cellular Biology, University of Arizona, Tucson, AZ 85721, USA

[†]Current address: Imanis Life Sciences, Rochester, MN 55901, USA

[§]Current address: National Biodefense Analysis and Countermeasures Center, Fort Detrick, MD 21702, USA

[¶]Current address: PPD, Inc., 929 N Front St. Wilmington, NC 28401, USA

***Correspondence:** fgoodrum@arizona.edu

Summary

Liver X receptor (LXR) signaling broadly restricts virus replication; however, the mechanisms of restriction are poorly defined. Here, we demonstrate that the LXR-inducible cellular E3 ligase IDOL (inducible degrader of low-density lipoprotein receptor, LDLR) targets the human cytomegalovirus (HMCV) UL136p33 protein for turnover. *UL136* encodes multiple proteins that differentially impact latency and reactivation. UL136p33 is a determinant of reactivation. UL136p33 is targeted for rapid turnover by the proteasome and its stabilization by mutation of lysine residues to arginine results in a failure to quiet replication for latency. We show that IDOL targets UL136p33 for turnover, but not the stabilized variant. IDOL is highly expressed in undifferentiated hematopoietic cells where HCMV establishes latency, but is sharply downregulated upon differentiation, a stimulus for reactivation. We hypothesize that IDOL maintains low levels of UL136p33 for the establishment of latency. Consistent with this, knockdown of IDOL impacts viral gene expression in WT HCMV infection, but not in infection where UL136p33 has been stabilized. Further, induction of LXR signaling restricts WT HCMV reactivation from latency, but does not affect replication of a recombinant virus expressing a stabilized variant of UL136p33. This work establishes the UL136p33-IDOL interaction as a key regulator of the bistable switch between latency and reactivation. It further suggests a model whereby a key viral determinant of HCMV reactivation is regulated by a host E3 ligase and acts as a sensor at the tipping point between the decision to maintain the latent state or exit latency for reactivation.

Importance

Herpesviruses establish life-long latent infections, which pose an important risk for disease particularly in the immunocompromised. Our work is focused on the beta-herpesvirus, human cytomegalovirus (HCMV) that latently infects the majority of the population worldwide. Defining the mechanisms by which HCMV establishes latency or reactivates from latency is important to controlling viral disease. Here, we demonstrate that the cellular inducible degrader of low-density lipoprotein receptor, IDOL, targets a HCMV determinant of reactivation for degradation. The instability of this determinant is important for the establishment of latency. This work defines a pivotal virus-host interaction that allows HCMV to sense changes in host biology to navigate decisions to establish latency or replicate.

Introduction

Viral latency, the ability of a virus to persist indefinitely in the infected host, is a hallmark of herpesviruses. Latency is defined as a non-replicative state punctuated by sporadic reactivation events where the virus replicates productively for transmission. Human cytomegalovirus (HCMV) is a beta-herpesvirus that establishes latent infection in hematopoietic progenitor cells (HPCs) and cells of the myeloid lineage (1). Reactivation of HCMV from latency in the immunocompromised can result in life-threatening disease and is a particularly important risk factor in the context of stem cell and solid organ transplantation. The molecular mechanisms by which HCMV senses changes in the host to make decisions to maintain latency or reactivate from latency is important in developing novel strategies to control viral reactivation and subsequent CMV disease.

78 Latency is a complex multifactorial phenomenon dependent on viral determinants, host
79 cell intrinsic, innate, and adaptive responses, as well as host cell signaling and
80 chromatin remodeling (2). Current paradigms hold that HCMV reactivation is tightly
81 connected to hematopoietic cell differentiation (3-7) or inflammatory signaling (3, 8-10).
82 However, much remains to be understood about the precise host contributions and key
83 viral factors that navigate the entry into or exit from latency. We and others have defined
84 roles of *UL133-138* gene locus encoded within the UL*b*' region of the HCMV genome for
85 latency and reactivation. *UL138* is required for latency and the UL138 protein functions
86 by regulating cell surface receptor trafficking and signaling (11-14), innate immune
87 responses (15, 16) and also contributes to repression of viral gene expression (17).
88 *UL135*, by contrast, is required for reactivation from latency, functioning in part by
89 opposing the function of *UL138* (18-20). *UL136* is expressed as 5 protein isoforms that
90 have differential effects on the establishment of latency or reactivation. The largest,
91 membrane-associated isoforms, UL136p33 (UL136p33) and p26, are required for
92 reactivation, whereas the small, soluble isoforms are required for latency in both *in vitro*
93 and *in vivo* experimental models (21, 22). Importantly, UL136 proteins accumulate with
94 delayed kinetics relative to UL135 and UL138 and maximal accumulation of *UL136*
95 gene products depend on the onset of viral DNA synthesis and/or entry into late phase.
96 Given its kinetics and dependence on viral DNA synthesis for maximal expression, we
97 postulate that UL136 may negotiate checkpoints that function to maintain latency or
98 commitment to reactivation from latency. Identifying host pathways regulating these viral
99 determinants is key to defining the mechanistic basis by which HCMV senses and
100 responds to changes in host biology to maintain latency or reactivate.

101

102 The cellular environment the virus encounters upon infection undoubtedly plays
103 important roles in the establishment of latency with a host of restriction factors prepared
104 to silence the viral genome, as well as a transcriptional milieu that impacts viral gene
105 expression. As an example, we have shown that the cellular transcription factor early
106 growth response factor-1 (EGR-1) drives the expression of UL138 for the establishment
107 of latency (20, 23). As EGR-1 is required to maintain stemness in the bone marrow
108 niche and is highly expressed in undifferentiated hematopoietic cells (24), cells are
109 primed to drive the expression of UL138 for latency upon infection. However, HCMV
110 also regulates EGR-1 expression through the differential trafficking and turnover of the
111 host receptor tyrosine kinase, epidermal growth factor receptor (EGFR) upstream of
112 EGR-1 (11, 19, 20) and through direct targeting by microRNAs that promote reactivation
113 (23). Thus, HCMV has evolved a multi-pronged strategy to manipulate and utilized host
114 pathways to regulate its gene expression, hardwiring infection into host signaling
115 pathways. With regards to reactivation, activation of the major immediate early (MIE)
116 transcriptional unit, encoding the major transactivators for viral replication, is highly
117 dependent on host transcription factors in myeloid cells (25). Host transcription factors
118 CREB, FOXO3a and AP-1 are downstream of major signaling pathways, including Src,
119 PI3K/Akt, and MEK/ERK, and are important for re-expression of MIE genes (26-28).
120 Further, UL7 encodes a ligand that binds the cellular Fms-like tyrosine kinase 3 receptor
121 (Flt-3R) that when secreted upon reactivation activates PI3K/AKT and MAPK signaling
122 to prevent cell death and stimulate differentiation for reactivation (29, 30). Through its
123 co-evolution with the human host, the biology of HCMV infection has become tightly

124 intertwined with the biology its host, which reflects the complex mechanisms the virus
125 has evolved to “sense” and “respond” to changes in the cellular environment to
126 influence “decisions" to maintain latency or reactivate from latency.
127
128 Here we demonstrate that the largest isoform of UL136, UL136p33, is targeted for rapid
129 turnover relative to other UL136 protein isoforms and that its instability ($t_{1/2}$~1 h) is
130 important to the establishment of latency. We identified the LXR-inducible degrader of
131 low-density lipoprotein receptor (LDLR) IDOL (also known as myosin regulatory light
132 chain interacting protein or MYLIP), as the host E3 ligase that targets UL136p33 for
133 turnover. IDOL expression is induced by oxysterol activation of the liver X receptor
134 (LXR) (31) and is regulated through hematopoietic differentiation (32, 33). In addition to
135 LDLR, IDOL also targets VLDLR and ApoER-2 and, therefore, is an important
136 homeostatic regulator of intracellular cholesterol (31, 34-36). The targeting of UL136p33
137 by IDOL suggests that the virus has evolved to be responsive to changes in cellular
138 cholesterol in its commitment to reactivation. A model emerges whereby high levels of
139 IDOL maintains low levels of UL136p33 for the establishment of latency, and the
140 downregulation of IDOL by differentiation results in the accumulation of UL136p33 to
141 drive reactivation. Indeed, induction of IDOL results in increased turnover of UL136p33
142 and prevents reactivation of HCMV from latency, whereas depletion of IDOL increases
143 viral gene expression in hematopoietic cells. Our findings define UL133p33 is a key viral
144 determinant of HCMV reactivation that acts as a sensor at the tipping point between the
145 decision to maintain the latent state or exit latency for reactivation.
146

147 **Results**

148 **UL136p33 is unstable and is targeted for proteasomal degradation**

149 *UL136* is expressed as at least 5 co-terminal protein isoforms (Fig. 1A). These isoforms
150 are encoded by transcripts with unique 5' ends and have distinct roles in viral latency
151 and reactivation (21, 22). The largest of these isoforms is a 33-kDa protein (UL136p33)
152 that is required for replication in endothelial cells as well as reactivation from latency in
153 CD34+ HPCs and in humanized mice (21). Conversely, the two small isoforms p23 and
154 p19 suppress replication in endothelial cells and promote latency in CD34+ HPCs and
155 humanized mice (22). The diametric nature of the UL136 system presupposes
156 additional levels of control to coordinate and commit to one infection program over
157 another, thereby allowing for either optimal replication/reactivation or robust latency.
158 The UL136 isoforms, and particularly the full-length isoform UL136p33, are uniquely
159 labile and sensitive to mechanical lysis while being processed (22). Based on this, we
160 hypothesized that the concentration of some UL136 isoforms is regulated by increased
161 proteolysis, and that the instability of UL136p33 may be important to establishing or
162 maintaining latency.

163

164 To explore the possibility that UL136 isoforms have different stabilities, we analyzed the
165 levels of UL136 isoforms in infected fibroblasts treated with cycloheximide (CHX) to halt
166 protein synthesis. Cycloheximide treatment resulted in a striking loss of UL136p33, p25,
167 and p23, but not p26 or p19 (Fig. 1B, left panel). These results indicated differential
168 stability whereby UL136p33, p25, and p23 may be subject to more rapid turnover, while
169 other UL136 isoforms are relatively stable. Proteasome inhibition robustly rescued

170 UL136p33, p25, and p23 isoforms (Fig. 1B, right panel). Inhibition of the lysosome with
171 NH_4Cl had no effect on rescue of any of the UL136 isoforms; however, inhibition of both
172 the lysosome and proteasome showed a somewhat additive effect. Together, these
173 results indicate that the rapid turnover of UL136p33, p25, and p23 is regulated by the
174 proteasome.
175
176 To establish the kinetics of isoform turnover, we analyzed the decay of UL136 isoforms
177 in fibroblasts infected with TB40/E-*UL136*$_{myc}$ and treated with CHX at peak UL136
178 isoform expression (Fig 1C). UL136p33 decayed with a half-life of 1 h ($t_{1/2}$=1 h) and p25
179 exhibited a $t_{1/2}$=3 h, while all other isoforms were stable over the 6 h time course (Fig
180 1D). The p23 isoform accumulates to very low levels making the decay of this protein is
181 difficult to determine. The rapid decay of UL136p33 relative to the other isoforms, as
182 well as its significance in HCMV reactivation prompted us to focus on determining the
183 factor(s) contributing to its instability.
184
185 **Lysine to arginine mutations stabilize UL136p33**
186 UL136 has four lysine (K) residues (denoted by red lines in Fig. 1A), three of which lie
187 upstream of the transmembrane domain (TMD) and are unique to the p33 isoform. To
188 determine if the turnover of UL136p33 was regulated by ubiquitin-mediated proteolysis,
189 we substituted all lysine residues for arginine (R) through site-directed mutagenesis in
190 an expression vector encoding UL136p33 to generate *UL136p33*$_{myc}$*ΔK→R*. The p33$_{\Delta K \rightarrow R}$
191 mutant had a $t_{1/2}$=5 h, compared to ~1 h for UL136p33 following CHX treatment (Fig.
192 2A). This observation, together with the stabilization of UL136p33 by proteasomal

193 inhibition (Fig. 1B), suggests that UL136p33 turnover is regulated by ubiquitin-mediated
194 proteasomal decay. Further, the rapid turnover of exogenously expressed UL136p33
195 (Fig. 2A, left panel) indicates that UL136p33's degradation is not dependent on virus or
196 virus-induced factors.
197
198 To determine the importance of UL136p33 instability in infection, we introduced the
199 lysine to arginine mutations into the *UL136*$_{myc}$ gene within the bacterial artificial
200 chromosome clone of TB40/E (*UL136*$_{myc}$*ΔK→R*). We measured the relative rates of
201 decay in fibroblasts infected with either the parental *UL136*$_{\mathrm{myc}}$ or *UL136*$_{myc}$*ΔK→R* virus
202 and treated with CHX and observed that p33$_{\Delta K \rightarrow R}$ was stabilized during infection relative
203 to wild type UL136p33 (Fig. 2B). Interestingly, we stabilization of UL136p33 diminished
204 levels of UL136p26 and p25 isoforms by mechanisms that have yet to be determined.
205
206 We then performed multistep growth curves on fibroblasts infected with *UL136*$_{myc}$ or
207 *UL136*$_{myc}$*ΔK→R* to analyze the impact of stabilizing UL136p33 on virus replication. No
208 change in the kinetics or yield of viral growth was observed during the productive
209 infection in fibroblasts when UL136p33 is stabilized relative to the WT infection (Fig.
210 2C). This was not surprising since the UL136p33 isoform, while important for replication
211 in endothelial cells and CD34+ HPCs, is dispensable for replication in fibroblasts (21,
212 22). In summary, UL136p33 instability is the result of lysine-dependent, proteasomal
213 degradation and mutating lysine residues to arginine in *UL136* stabilizes the protein with
214 no effect on virus replication in fibroblasts.
215

216 Since UL136p33 is required for reactivation from latency in CD34+ HPCs (21), we
217 hypothesized that the instability of UL136p33 allows for a tunable concentration gradient
218 where low levels are important for the establishment of latency and accumulation past a
219 threshold is important for reactivation. To test this hypothesis, we performed a latency
220 assay in primary human CD34+ HPCs infected with the parental *UL136*$_{\text{myc}}$ or
221 *UL136*$_{myc}$*ΔK→R* viruses. *UL136*$_{myc}$-infected CD34+ HPCs generated >2-fold
222 frequencies of infectious centers following reactivation compared to the pre-reactivation
223 control (Fig. 2D). However, the pre- and post-reactivation frequencies of infectious
224 centers were not different in the *UL136*$_{myc}$*ΔK→R* infection and were almost two-fold
225 above *UL136*$_{\text{myc}}$ pre-reactivation. These results indicate that HCMV replication in
226 CD34+ HPCs is not quieted when UL136p33 is stabilized, and that this virus does not
227 establish a latent infection. In a separate study, we have shown that the stabilization of
228 UL136p33 results in increased virus replication (a failure to establish latency) in a
229 humanized mouse model of latency (37). As is the case with many viral proteins, UL136
230 isoforms, even with a myc epitope tag, are not expressed to detectable levels in
231 hematopoietic cells, and we have been unsuccessful in generating antibodies to UL136.
232 Nevertheless, given the requirement for UL136p33 for reactivation and replication in
233 CD34+ HPCs, the *UL136*$_{myc}$*ΔK→R* infection phenotype is consistent with accumulation
234 of UL136p33 beyond a threshold critical for commitment to replication.
235

236 **The host E3 ligase IDOL targets UL136p33 for proteasomal degradation**

237 Ubiquitination of cargo by E3 ligases is an important step in targeting a protein for
238 proteasomal degradation (38, 39). Because UL136p33 is rapidly turned over by the

239 proteasome even in the absence of infection and lysine to arginine substitutions
240 stabilized UL136p33, we hypothesized that a host E3 ligase targets UL136p33 for
241 turnover. We identified UL136 interacting proteins by a yeast two-hybrid screen (Y2H)
242 using the C-terminal region of UL136 (amino acids 141-240) as bait. Intriguingly, we
243 identified the host E3 ligase IDOL (**i**nducible **d**egrader **o**f **l**ow-density lipoprotein
244 receptor), also known as MYLIP, as a candidate host interactor of UL136 (Supporting
245 information, SI Table 1). IDOL induces the degradation of the low-density lipoprotein
246 receptor family members LDLR, VLDLR, and ApoER-2 (35, 36). The degradation of
247 these receptors is a physiological response to increased cholesterol, which is modified
248 to oxysterols that activate the LXR transcription factor to induce *IDOL* expression (36,
249 40, 41).
250
251 To determine if IDOL targets UL136p33, we analyzed the ability of IDOL to interact with
252 and impact UL136p33 levels. We validated the interaction between IDOL and
253 UL136p33 by immunoprecipitating (IP) UL136p33-IDOL complexes from cells
254 transiently overexpressing myc-tagged UL136p33 or HA-tagged IDOL. Transient
255 overexpression is necessary due to the lack of commercially available antibodies
256 specific and sensitive enough to detect or immunoprecipitate endogenous IDOL.
257 Pulldown of $IDOL_{HA}$ or $p33_{myc}$ coprecipitated the alternant partner (Fig. 3A), confirming
258 the interaction between UL136p33 and IDOL. Further analysis indicated that co-
259 expression of IDOL with UL136p33 resulted in a ~60% reduction in UL136p33 levels
260 compared to when UL136p33 was co-expressed with an empty vector (Fig. 3B top and
261 quantified in Fig. 3C), consistent with IDOL driving UL136p33 turnover. By contrast,

262 $p33_{\Delta K \rightarrow R}$ levels were not affected by IDOL co-expression (Fig. 3B bottom and quantified
263 in Fig. 3C), in agreement with the hypothesis that ubiquitination on lysine residues is
264 required for UL136p33 turnover via the proteasome. Taken together, IDOL functions as
265 a host E3 ligase that targets UL136p33 for proteasomal degradation.
266
267 We next induced endogenous IDOL expression with an LXR agonist GW3965 or LXR-
268 independent agonist HBX41-108 in cells transiently expressing UL136p33 or $p33_{\Delta K \rightarrow R}$.
269 Because endogenous IDOL cannot be detected by western blot using available
270 antibodies (34, 42, 43), the induction of IDOL was verified by the loss of its target
271 ApoER-2 (Fig. 3D). Induction of IDOL, by both GW3965 and HBX41-108 resulted in a
272 reduction of UL136p33 (Fig. 3D, top), but not $p33_{\Delta K \rightarrow R}$ (Fig. 3D, bottom). These results
273 further confirm that endogenous IDOL targets UL136p33 for ubiquitin-dependent
274 degradation.
275
276 The Y2H bait was composed of the C-terminal region of UL136 spanning amino acids
277 141-240 downstream of the predicted transmembrane domain. These residues are
278 shared by all the UL136 isoforms (Fig. 1A). Further, our data indicated that p25 and p23
279 proteins are also labile following CHX treatment and these smaller isoforms could be
280 rescued, like UL136p33, by inhibiting the proteasome (Fig. 1B, right panel). The p25
281 and p23 isoforms have a single lysine which is located downstream of the TMD in the
282 full length UL136 isoform (Fig. 1A). Transient co-expression of IDOL with either p25 or
283 p23 did not lead to any notable turnover of these proteins (Fig. 3E-G). These data
284 collectively led us to conclude that IDOL specifically targets UL136p33 for turnover, and

285 it does not mediate the degradation of p25 and p23. The mechanism by which p25 and
286 p23 are turned over remains to be elucidated and could reflect differential trafficking and
287 localization of the proteins (22).
288
289 To further define the specificity of IDOL-mediated turnover of UL136p33, we co-
290 expressed UL136p33 with another E3 ligase, Cbl. Cbl targets tyrosine kinase receptors,
291 such as EGFR, for ubiquitination and subsequent degradation by the lysosome (44).
292 Levels of UL136p33 were unaffected by co-expression with Cbl (Fig. 3H-I), indicating
293 some specificity of IDOL for proteasomal turnover of UL136p33.
294
295 **IDOL impacts UL136p33 protein levels in HCMV-infected primary fibroblasts**
296 In the context of a productive infection in fibroblasts, we found that infection with either
297 the parental $UL136_{myc}$ or $UL136_{myc}\Delta K\rightarrow R$ induced *IDOL* transcripts by at least 5-fold
298 compared to mock-infection by reverse transcriptase, quantitative PCR (RT-qPCR),
299 (Fig. 4A). *IDOL* transcript upregulation was sustained over time during infection and
300 peaked at close to 10-fold by 3 dpi. No changes in *IDOL* transcript levels were detected
301 in mock controls over the same time-course. Because *IDOL* induction is a consequence
302 of increased cellular cholesterol, we measured cholesterol content in infected cells to
303 correlate it to the upregulation of *IDOL* transcripts. Using this approach, we noted that
304 HCMV increased cholesterol concentration by at least 29% from 1 dpi onward (Fig. 4B),
305 consistent with previous findings on HCMV-modulation of lipid biosynthesis (45-50).
306 Taken together, infection in fibroblasts upregulates expression levels of IDOL
307 transcripts, which is correlated with increased intracellular cholesterol levels.

308

309 To address the effect of HCMV-mediated induction of IDOL on UL136p33 levels in a
310 productive infection, we again induced IDOL expression with the LXR agonist GW3965
311 or HBX41-108 in TB40/E-*UL136*$_{myc}$- or -*UL136*$_{myc}$ΔK→R-infected fibroblasts. IDOL
312 induction resulted in a 50% reduction in the levels of UL136p33 but did not significantly
313 affect p33$_{\Delta K \rightarrow R}$ levels (Fig. 4C and D). Diminished levels of smaller UL136 isoforms are
314 again apparent in the *UL136*$_{myc}$ΔK→R infection. We next disrupted *IDOL* expression in
315 fibroblasts to answer the question whether IDOL depletion would rescue UL136p33
316 turnover. CRISPR-mediated knockout (KO) of *IDOL* using guide RNAs to disrupt all the
317 isoforms of IDOL was validated by Sanger sequencing and increased ApoER-2 as a
318 proxy for *IDOL* KO (Fig. 4E). Further, CRISPR KO of *IDOL* had no effect on HDAC1, a
319 potential off-target hit when knocking out *IDOL*. In fibroblasts depleted of IDOL,
320 UL136p33 levels increased at 2 and 3 dpi compared to luciferase KO controls, but did
321 not affect levels of p33$_{\Delta K \rightarrow R}$ (Fig. 4F and quantified in 4G). Further, IE2 levels were also
322 significantly increased in IDOL KO cells infected with *UL136*$_{myc}$, but not changed by
323 IDOL KO in the *UL136*$_{myc}$*ΔK→R* infection (Fig. 4H). Together, these results indicate that
324 IDOL regulates UL136p33 concentration, which indirectly impacts IE expression in the
325 context of infection.

326

327 **LXR induction and IDOL restricts HCMV gene expression and reactivation in**
328 **models of latency**

329 HCMV latency is studied in a variety of models. Due to limitations inherent to each
330 model, there is no perfect model and, therefore, we explore latency questions using

331 multiple complementary models. To explore the role of IDOL in regulating UL136p33
332 levels in latency and reactivation, we have used two models of HCMV: (1) THP-1 cell
333 line model and (2) CD34+ primary HPC model. In the THP-1 monocytic cell line model,
334 cells are infected in an undifferentiated state for the establishment of latency. Viral gene
335 expression is detected early (1 dpi) following infection but is silenced as the virus
336 establishes a latent-like state (51). Re-expression of viral genes for reactivation is
337 stimulated by differentiating the cells into macrophages with a phorbol ester,
338 tetradecanoylphorbol acetate (TPA) (52-57). This is a strong model for looking at
339 transcriptional changes associated with latency and reactivation; however, this model is
340 limited in that THP-1 cells do not robustly or consistently support viral genome synthesis
341 or production of viral progeny following TPA induction, a requirement for bona fide
342 reactivation. The gold-standard for HCMV latency is the ability of the virus to establish
343 and reactivate from latency in primary human CD34+ HPCs (58). In contrast to THP-1
344 cells, the primary CD34+ HPC model supports viral genome synthesis and the formation
345 of infectious progeny in response to reactivation. However, the model is limited by
346 substantial donor-variability associated with primary human cells, heterogeneity of the
347 population, the availability of cells in numbers to provide sufficient starting material for
348 many assays, and the ability to manipulate these cells (e.g. gene knockdowns or
349 overexpression) without affecting their differentiation or quantities sufficient for HCMV
350 infection assays. Further, because reactivation of HCMV from CD34+ HPCs occurs at
351 low frequency (1 in ~9,000 cells), analysis of molecular events associated with
352 reactivation is challenging. The use of both models yields complementary insights into

353 the patterns of gene expression upon infection or reactivation (THP-1) and virus
354 production (CD34+ HPCs) to understand latency and reactivation.
355
356 Dynamic gene expression changes are associated with monocyte-to-macrophage
357 differentiation (32, 59, 60). Because IDOL is highly expressed in bone marrow (61), we
358 hypothesized that *IDOL* expression may be dictated by the differentiation state of the
359 cell and would regulate UL136 levels in a differentiation-dependent manner. Indeed, we
360 found that *IDOL* was highly expressed in undifferentiated THP-1 monocytes prior to
361 infection but was sharply downregulated upon THP-1 cell differentiation (Fig. 5A).
362 Further, while no significant differences in *IDOL* expression were observed between
363 uninfected cells and $UL136_{myc}$ infection, $UL136_{myc}\Delta K\rightarrow R$ infection significantly reduced
364 *IDOL* expression in the undifferentiated, latent phase (Fig. 5A). This result suggests that
365 UL136p33 levels may feedback to impact IDOL expression in a cell type-dependent
366 manner.
367
368 To determine how IDOL impacts HCMV infection in hematopoietic cells, we knocked out
369 *IDOL* in THP-1 cells using CRISPR. The knockdown was validated using an ELISA
370 assay for the detection of IDOL protein (Fig. 5B); IDOL protein was reduced in
371 undifferentiated cells to levels induced by differentiation. Further, *IDOL* KO had no off-
372 target effects on HDAC1 (Fig. 5C). Given the challenges of detecting UL136 isoforms,
373 particularly in hematopoietic cells, we examined IE1, IE2 and UL135 gene expression
374 as proxies for determining the effect of *IDOL* KO on infection in THP-1 cells. UL135 and
375 IE1/2 proteins are detected early during infection in THP-1 cells but diminish as the

376 virus establishes latency between 3 and 5 dpi (Fig. 5D-E) (52). *IDOL* KO resulted in an
377 increased initial burst in the expression of IE1, IE2, and UL135 at 1 dpi relative to
378 control *Luc* KO cells in *UL136*$_{\text{myc}}$ infection. Notably, the major HCMV transactivator, IE2,
379 was detected in *UL136*$_{myc}$ infection in the IDOL KO condition, but not in the *Luc* KO
380 control. The increased viral gene expression in the IDOL KO is consistent with
381 increased viral activity. However, gene expression was still relatively quieted by 5 dpi,
382 suggesting that induction of IDOL does not fully prevent the silencing of viral gene
383 expression in this system and that other viral or cellular factors are required. As we
384 have never identified a condition or mutant virus that is not ultimately silenced in THP-1
385 cells, this is not unexpected and it may reflect the robust program for restriction and
386 silencing in THP-1, indicated by the inability of these cells to support viral DNA
387 synthesis and progeny formation even with TPA treatment. UL135 and IE1, as well as
388 IE2, were detected in *UL136*$_{myc}$*ΔK→R* infection of THP-1 cells. Importantly, *IDOL* KO
389 had no effect on IE1, IE2, or UL135 expression in *UL136*$_{myc}$*ΔK→R* infection (Fig. 5D-E),
390 consistent with a role for IDOL in regulating the establishment of latency by targeting
391 UL136p33 for turnover. In contrast to *UL136*$_{\text{myc}}$ infection, IE2 was detected in all
392 conditions of the *UL136*$_{myc}$*ΔK→R* infection and is not increased further by IDOL KO.
393 While a potent transactivator, IE2 feeds back to negatively regulate the major immediate
394 early promoter and its own expression (62-65). The differences in IE2 expression in
395 IDOL KO in *UL136*$_{\text{myc}}$ and *UL136*$_{myc}$*ΔK→R* infection may reflect complexities in the
396 regulation of IE gene expression or the possible dysregulation and loss of middle UL136
397 isoforms in *UL136*$_{myc}$*ΔK→R* infection (Fig. 2). Further work is required to understand
398 this relationship. These results indicate that loss of IDOL increases viral gene

399 expression in *UL136*$_{myc}$ infection at least at early times following infection of THP-1
400 cells, suggesting a role for IDOL in regulating HCMV infection in undifferentiated THP-1
401 cells. This finding reflects IDOL-induced changes in UL136p33 since the stabilized
402 variant does not differentially express genes in an IDOL-dependent manner. This
403 finding is consistent with a role for IDOL in driving instability of UL136p33 and the role of
404 UL136p33 in driving HCMV replication in hematopoietic cells (66). Further, these data
405 indicate that UL136p33 may negatively regulate IDOL expression in hematopoietic cells,
406 as the stabilized form of UL136p33 results in greater repression of IDOL transcripts by
407 HCMV infection.
408
409 To further explore the importance of IDOL in latency, we turned to the primary CD34+
410 HPC experimental model (58). IDOL is expressed in undifferentiated CD34+ HPCs and,
411 similar to our findings in the THP-1 cell model, its expression is downregulated by
412 differentiation (Fig. 6A). Further, the LXR-agonist GW3965 induces IDOL expression in
413 either infected or uninfected CD34+ HPCs (Fig. 6B). To measure the impact of LXR
414 induction on reactivation in primary CD34+ HPCs, we isolated CD34+ HPCs infected
415 with TB40/E-*UL136*$_{myc}$ or -*UL136*$_{myc}$*Δ*K→R (GFP+) by fluorescent activated cell sorting
416 and seeded the cells into long-term bone marrow cultures. To analyze infectious virus
417 production, infected CD34+ HPC cultures were split at 10 dpi. Half the cells were
418 seeded by limiting dilution into co-culture with fibroblasts and cytokine-rich media to
419 stimulate reactivation from latency. The other half was mechanically lysed and lysates
420 were seeded by limiting dilution onto fibroblast monolayers to determine the virus
421 present prior to reactivation (pre-reactivation). Relative to the DMSO control, GW3965

422 treatment restricted *UL136*$_{myc}$ reactivation (Fig. 6C), consistent with a requirement for
423 accumulation of UL136p33 for reactivation. By contrast, *UL136*$_{myc}$*ΔK→R* did not
424 establish latency and LXR induction, and presumably increased levels of IDOL, did not
425 restrict replication of *UL136*$_{myc}$*ΔK→R.* Given the limited availability of human CD34+
426 HPCs, data from two independent donors are shown for figure 6C. These results are
427 consistent with the model that IDOL restricts virus reactivation in a manner dependent
428 on its ability to turnover UL136p33 since LXR induction has not effect of the infection
429 the *UL136*$_{myc}$Δ*K→R*. Taken together with the THP-1 experiments, these results suggest
430 that IDOL-driven UL136p33 instability is required for latency and that induction of IDOL
431 suppresses reactivation, presumably through suppressing the accumulation of
432 UL136p33 (Fig. 7).
433

434 **Discussion**

435 Latent viruses require mechanisms to sense the cellular environment, filter noise and
436 respond to host cues to maintain a quiescent latent state or to reactivate replication (1).
437 While the decision to enter or exit latency is often depicted as a simple binary on/off
438 switch, the reality is more likely that a number of successive checkpoints must be
439 crossed, each requiring thresholds in viral or cellular activities to be reached in making
440 the commitment to productive reactivation. Developing strategies to control entry into or
441 exit from HCMV latency and ultimately control CMV disease rests upon identifying the
442 virus-host interactions that govern the decisions around latency and reactivation. Here
443 we demonstrate the existence of an unstable viral determinant of reactivation,
444 UL136p33 (Fig. 1) and that its instability is important for the establishment of latency in

445 CD34+ HPCs (Fig. 2). We demonstrate that its instability is dependent upon a host E3
446 ligase, IDOL, which is regulated by hematopoietic differentiation (Fig. 3). Knockdown of
447 IDOL levels increases viral gene expression (Fig. 4) and LXR induction restricts
448 replication in hematopoietic models of latency (Fig. 5-6). Our results support a model,
449 rich in hypotheses for further investigation, whereby UL136p33 is maintained at low
450 levels for the establishment of latency because IDOL levels are high (Fig. 7). Upon
451 differentiation, IDOL levels fall (Fig. 5A and 6A), allowing UL136p33 levels to rise, which
452 facilitates HCMV crossing at least one threshold towards reactivation. UL136p33
453 accumulation is amplified and re-enforced by the onset of viral DNA synthesis and entry
454 into late phase (22) and high levels of UL136p33 further suppresses IDOL expression
455 (Fig. 5A). These findings define novel virus-host interactions that govern entry into and
456 exit from latency. Moreover, these findings suggest that by utilizing IDOL to regulate
457 levels of a critical viral determinant for reactivation, the virus evolved to hardwire this
458 decision into LXR signaling, which ultimately controls IDOL levels. Future work will
459 define the mechanisms by which UL136 regulates HCMV infection and commitment to
460 replication in hematopoietic cells. Understanding the relationship between UL136
461 isoforms, to other *UL133-UL138* locus- encoded proteins and to host interactors will be
462 critical to mechanistic insights.
463
464 *IDOL* is transcriptionally upregulated by excess cholesterol derivatives (oxysterols) that
465 are sensed by LXR and in a cell type-dependent manner (36, 67-70). RNA sequencing
466 to classify the tissue-specific expression of genes across a representative set of all
467 major human organs and tissues revealed that IDOL is highly expressed in the bone

468 marrow, where CD34+ HPCs and monocytes are generated (71). The level of IDOL
469 expression in the BM is only second to the placenta. High expression of IDOL in
470 undifferentiated progenitor cells (Fig. 6A) or in monocytes (Fig. 5A) suggests they are
471 intolerant of high cholesterol levels. Consistent with this, undifferentiated THP-1
472 monocytes express significantly higher levels of cholesterol efflux genes, such as
473 CES1, and express significantly lower levels of influx genes (72). By contrast, THP-1
474 monocyte-derived macrophages upregulate cholesterol influx genes, such as scavenger
475 receptor A1 (SR-A1) and CD36 to become lipid-loaded macrophages or foam cells.
476 Further, statin treatment to lower cholesterol reduces CD34+ HPC populations in the
477 circulation and high cholesterol promotes CD34+ HPC proliferation, myelopoiesis as
478 well as monocyte and granulocytic differentiation (73-75). While carefully designed
479 studies are required to understand how statins specifically affect HCMV latency and/or
480 reactivation, these findings suggest the possibility that sterol homeostasis impacts
481 HCMV latency and reactivation. Untreated hypercholesterolemia might lead to
482 increased hematopoietic differentiation and a higher frequency of HCMV reactivation
483 events, whereas statin treatments may restrict HCMV reactivation and replication. Given
484 the role demonstrated here for IDOL in the regulation of cholesterol and UL136p33
485 expression, the high levels of IDOL expression make progenitor cells an ideal
486 environment for HCMV latency in which UL136p33 is suppressed by rapid turnover. It is
487 intriguing to speculate a possible role of UL136p33 as a viral sensor of changes in LXR
488 signaling compatible with reactivation.
489

490 HCMV infection remodels the cellular lipid metabolic landscape by upregulating *de novo*
491 cholesterol biosynthesis during a productive infection (46, 49, 50). It is, therefore,
492 expected that HCMV infection would induce IDOL expression during a replicative
493 infection. While IDOL and cholesterol are induced by infection in fibroblasts (SI Fig. 2A-
494 B), IDOL expression was not induced by infection in hematopoietic cells. In fact, IDOL
495 expression was downregulated by *UL136*$_{myc}$Δ*K→R* infection (Fig. 5A). This disparity in
496 the regulation of IDOL likely reflects cell type-specific differences, including tolerance for
497 cholesterol and differences in the nature of the infection in each cell. While cholesterol
498 increases in macrophage cells, they also have higher tolerance to cholesterol than
499 HPCs or monocytes (76-78). Accordingly, despite increased cholesterol in
500 macrophages, IDOL levels are strikingly downregulated in THP-1 cells induced to
501 differentiate with TPA (Fig. 5A) or CD34+ HPCs are induced to differentiate with
502 cytokines (Fig. 6A).
503
504 IDOL recognizes a conserved FERM domain (WxxKNxxSI/MxF) within the cytoplasmic
505 tail of its targets (ApoER-2, LDLR and VLDLR), to mediate ubiquitination for lysosomal
506 degradation (31, 35, 36, 79). Canonical IDOL targets reside at the plasma membrane
507 and are typically internalized via the endocytosis and trafficked to the lysosome (79). By
508 contrast, UL136p33 is predominantly Golgi-associated (22), lacks a FERM domain, and
509 is degraded via the proteasome (Fig. 1B). Differences in localization and trafficking
510 pathways between natural IDOL targets and UL136p33 may differentially direct the
511 degradation pathway. It remains to be determined how IDOL recognized and targets
512 UL136p33, but it is possible that the two proteins interact indirectly.

513

514 Activation of LXR in human foreskin fibroblasts with GW3965 prior to HCMV infection
515 has been shown to depress expression levels of viral proteins, such as IE2, pp28, pp65
516 and gB (80). GW3965 treatment is also reported to induce IFN-γ (81), a cytokine which
517 directly inhibits IE1/2 mRNA expression (82). These findings suggest the possibility that
518 the effects of LXR agonists on UL136p33 levels are due to a global repression of viral
519 gene expression. However, our results argue against this scenario. First, we observed
520 no effect on IE gene expression at 2 dpi in infected fibroblasts treated with GW3965 or
521 HBX41-108 (Fig. 4C-D), consistent with the attenuation of IFN-γ at later times (83).
522 Second, specific depletion of *IDOL* increases UL136p33, consistent with IDOL-specific
523 effects on UL136p33 levels. Nevertheless, to avoid this potential pitfall, we treated cells
524 in our experiments with these agonists following the establishment of infection and IE
525 gene expression in our studies.

526

527 The LXR axis is important for the biology of other herpesviruses. A recent report
528 demonstrates that the alpha herpesvirus pseudorabies virus (PRV), etiologic agent of
529 the economically important Aujeszky's disease, has evolved to inhibit LXR at both
530 transcription and protein levels (84). Using an inverse LXR agonist SR9243, Wang and
531 colleagues showed that inhibiting LXR increased PRV replication, whereas 3 different
532 LXR agonists and the oxysterol 22R-hydroxycholesterol all inhibited PRV replication
533 (84). However, PRV can be rescued from the suppressive effects of an LXR agonist by
534 supplementing with cholesterol (84), consistent with a viral need for cholesterol to
535 replicate. LXR also inhibits the murine gamma herpesvirus MHV68 as it replicates better

536 in *LXR*$^{-/-}$ macrophages and, contrary to PRV, MHV68 infection increases LXRα (85).
537 Importantly, LXRα restricts reactivation of MHV86 in peritoneal cells, but not in
538 splenocytes (86). The cell type-dependent role of LXR signaling for reactivation
539 suggests the possibility that a LXR signaling might control a MHV68 determinant of
540 reactivation in peritoneal cells that is dispensable in splenocytes. Similarly, disruption of
541 or stabilization of UL136p33 has no impact on replication in fibroblasts (Fig. 2C) (22),
542 but strongly impacts replication in HPCs (Fig. 2D) and endothelial cells (21). Viral
543 factors encoded by MHV68 and regulated by LXR signaling have yet to be determined.
544
545 In addition to herpesviruses, LXR signaling suppresses the replication of other viruses,
546 including Hepatitis C Virus (HCV) (87, 88), human immunodeficiency virus (HIV) (89-
547 91), and Newcastle disease virus (NDV) (92). Intriguingly, activation of LXR signaling
548 suppresses hepatitis C virus (HCV) replication in an IDOL-dependent manner. The
549 suppression of HCV is presumably due to the requirement of LDLR for an entry receptor
550 since once infection is established, IDOL induction does not seem to have an effect on
551 HCV replication (93). However, there are mixed reports on the requirement for LDLR for
552 HCV entry or its specific function in HCV replication (94-96).
553
554 While many host pathways are implicated in the regulation of herpesvirus latency, the
555 interplay between viral determinants and their regulation by host mechanisms to
556 terminate activity is less well appreciated, particularly for HCMV. The expression of
557 HSV-1 ICP0, a critical protein for reactivation and replication, is suppressed by the host
558 neuronal microRNA-138 to facilitate latency (97, 98). Moreover, ICP0 was recently

559 shown to be regulated by the host E3 ligase, TRIM23, which is in turn, countered by the
560 HSV-1 late protein, $\gamma_1$34.5 (99). While speculative, TRIM23 may moderate ICP0 protein
561 levels to suppress reactivation, where $\gamma_1$34.5 ensures the commitment to replication by
562 blocking TRIM23-mediated turnover of ICP0. Further, the E3 ubiquitin ligase, MDM2,
563 restricts levels of the Kaposi's sarcoma-associated herpesvirus (KSHV) transactivator,
564 RTA/ORF50, acting as pro-viral factor for latency (100). RTA/ORF50 in turn induces
565 degradation of vFLIP through the host Itch E3 ubiquitin ligase to attenuate vFLIP-driven
566 NFκB signaling for reactivation (101, 102). Coopting and regulating host E3 ligases to
567 target viral proteins for latency allows infections to respond quickly to host cues (e.g.,
568 prior to changes requiring transcription of genes and translation of proteins) for
569 reactivation. Further, it will be important to determine if UL136p33 feeds back to
570 regulate *IDOL* expression based on the observation that stabilization of UL136p33
571 represses *IDOL* expression in undifferentiated THP-1 cells (Fig. 5A). It will be important
572 to further define the mechanisms by which UL136p33 interacts with host pathways to
573 impact viral gene expression and promote context-dependent replication and
574 reactivation.
575
576 The evolution of viruses to depend on host factor-mediated turnover of critical viral
577 determinants is shared across highly divergent systems. Bacteriophages establish a
578 dormant lysogenic state to cope with their variable and unpredictable environment
579 (103). Bacteriophage λ lysogeny depends on the competition between repressors and
580 activators of gene expression that serve as a gatekeeper for the lytic pathways (104,
581 105). As a primary example, competitive binding of the lysogeny determinant CI and the

582 immediate early gene Cro at regulatory operator elements puts CI-Cro at the heart of a
583 bistable switch controlling lysogenic-lytic decisions. Another determinant, CII, is
584 expressed with later kinetics and is also critical to the commitment to lysogeny (106,
585 107). CII promotes expression of CI while it represses expression of the anti-terminator
586 Q, that must accumulate to a threshold to drive lytic gene expression. Critical effectors
587 in bacteriophage lysogeny, such as CI and CII, are susceptible to destruction by host
588 proteases that are induced in response to stresses, such as DNA damage (108, 109).
589 Similar to the model emerging for UL136-IDOL interaction in regulating a determinant of
590 reactivation for latency, the decision to establish lysogeny depends on the accumulation
591 of lysogenic effectors and is responsive to host determinants regulated by
592 environmental cues. Further, while CI is robust, the expression of CII, like UL136, is
593 sensitive to genome copy number or other fluctuations in the system, providing
594 additional checkpoints in regulating the decision.
595
596 With respect to the system emerging for HCMV, the *UL133-UL138* locus coordinates
597 the expression of multiple genes impacting infection fate decisions. While UL135 and
598 UL138 are not known to directly regulate gene expression, their opposing impact on
599 host EGFR/PI3K signaling (11, 18, 20) has parallels to the Cro-CI bistable genetic
600 switch. Further, UL136p33 is expressed with later kinetics than the UL135/UL138
601 determinants, and robust UL136p33 expression is dependent on crossing a threshold of
602 commitment to viral DNA synthesis (22). In addition, UL136p33 is remarkably unstable
603 compared to other *UL133-UL138* genes and other UL136 isoforms, and, as we have
604 shown here, its instability is dependent upon a host E3 ligase regulated by

605 differentiation-linked changes in IDOL expression. Although the UL136p33 protein is
606 undetectable in THP-1 monocytes or hematopoietic cells, KO of *IDOL* increases
607 expression of genes critical for replication (e.g., IEs and UL135) and stabilization of
608 UL136p33 results in a virus that replicates in the absence of a stimulus for reactivation
609 in vitro (Fig. 2D), but also in a humanized mouse model of latency (37). While UL135 is
610 critical for overcoming the repressive effects of UL138 for successful reactivation, we
611 assert that the subsequent accumulation of UL136p33 beyond a threshold is also
612 important for commitment to the replicative state (Fig. 7). It is important to understand
613 the relationship between UL135 and UL136p33 in the commitment to HCMV
614 reactivation (37) since as both are required for reactivation and how latency-promoting
615 UL136p23/19 isoforms (21) may contribute to the establishment of latency or counter
616 the progression towards reactivation to maintain a latent infection. This is a particularly
617 intriguing question as the stabilization of UL136p33 not only affects levels of IDOL
618 mRNA, but also affects levels of other UL136 isoforms (Fig. 2B). Finally, these findings
619 indicate that the LXR-IDOL axis may be a potential target for controlling HCMV
620 reactivation clinically.
621

622 **Methods**

623 **Yeast two-hybrid screen**

624 A yeast screen for human cellular interacting proteins of pUL136 was performed using the
625 Matchmaker Gold Yeast Two-Hybrid System (Clontech) and the Mate and Plate Universal
626 Human Library (Clontech). This yeast two-hybrid universal library was constructed from human
627 cDNA that has been normalized to remove high copy number cDNAs (overrepresented
628 transcripts) to facilitate the discovery of low copy number novel protein-protein interactions. All

629 protocols were carried out according to the manufacturer's guidelines. Yeast dual transformation
630 and yeast mating was performed according to established protocols from Clontech. Yeast prey
631 vectors were isolated from Y187 yeast and subsequently transformed into DH10B *E. coli*. After
632 selection for *E coli* containing yeast prey vectors, the plasmids were isolated and sequenced to
633 identify interacting partners. Candidate interactors are listed on SI Table 1.
634

635 **Cells and viruses**

636 Human primary embryonic fibroblasts (MRC-5; ATCC) and human kidney embryonic
637 293T (HEK 293T; ATCC) cells were maintained in Dulbecco's Essential Media (DMEM).
638 The DMEM was supplemented with 10% fetal bovine serum (FBS), 10 mM HEPES, 1
639 mM sodium pyruvate, 2 mM l-alanyl-glutamine, 0.1 mM nonessential amino acids, 100
640 U/ml penicillin, and 100 µg/ml streptomycin. CD34+ hematopoietic progenitor cells
641 (HPCs) were isolated from de-identified medical waste following bone marrow isolations
642 from healthy donors for clinical procedures at the Banner-University Medical Center at
643 the University of Arizona (58). THP-1 cells were maintained in RPMI1640 (Gibco)
644 supplemented with 10% FBS, 1 mM sodium pyruvate, 0.1 mM β-mercapto-ethanol
645 (Sigma).
646

647 The wild type TB40E/05 strain expressing GFP as a marker for infection (110) was
648 engineered to fuse the myc epitope tag in frame at the 3' end of *UL136* (*UL136*$_{myc}$ virus)
649 using BAC recombineering as described previously (22). The *UL136*$_{myc}$*ΔK→R* virus was
650 constructed following methods previously described (22). For generation of
651 *UL136*$_{\mathrm{myc}}$ΔK→R, *UL136*$_{myc}$*ΔK→R* pGEM-T Easy construct was created by site-directed
652 Phusion mutagenesis according to the manufacturer's instruction (New England

653 Biolabs). Inverse PCR was used to mutagenize lysines 4, 20, 25, and 113 to arginine
654 using the primers: 5'-GACGTTGGAAATAGATGGCGGCGTCGAAGGCCCTGAGTCGC-
655 3' (forward); CAAGTCCCACGTCATTTCTGGCATCTCCACGCCCCTGACTGACAT-3'
656 (reverse) for the first 3 lysine residues in the N-terminal region and 4th lysine was
657 mutagenized to arginine with the forward primer 5'-
658 ACGAGCGGCAGAGAAGCAGACGGC-3', and reverse primer
659 GGTGCCGACGGCACCTCTCAGGATAATG-3'. Following verification by Sanger
660 sequencing, a region of the *UL136K-Rmyc* pGEM-T Easy was PCR amplified from bp
661 854 of UL135 [UL135(bp854)] to UL138 (bp139). This PCR product was gel purified and
662 recombined with a ΔUL136<GalK> BAC as previously described (22). BAC integrity was
663 tested by enzyme digest fragment analysis and sequencing of the UL133/8 viral
664 genomic region. All BAC genomes were maintained in Escherichia coli SW102, and
665 viral stocks were propagated by transfecting 15 to 20 µg of each BAC genome, along
666 with 2 µg of a plasmid encoding UL82 (pp71), into 5 × 106 MRC-5 fibroblasts and
667 subsequently purified and stored as previously described (22).
668

669 **Immunoblotting**

670 Cells were washed twice in PBS (Gibco) and lifted from cell culture vessels with 0.25X trypsin
671 (Gibco). Cells were washed in cold PBS, pelleted at 1000 xg for 2 minutes followed by storage
672 at -80 ^{o}C before lysis in RIPA buffer. Total protein was quantified using a BCA assay and 50 µg
673 of each sample was prepared for loading onto 12% precast PAGE gels (GenScript). Wet
674 transfers were performed onto 0.45 uM pore-sized PVDF membranes (Immobilon). Blocking
675 was achieved by 5% skimmed milk in 1X TBST, or 5% BSA in 1X TBST. Primary and
676 secondary antibodies used for western blot analyses are indicated in Table 1.

677

678 **Table 1. Antibodies used in this study**

Antibodies		
Rabbit monoclonal anti-ApoER-2	Abcam	Cat#ab108208
Rabbit polyclonal anti-FLAG tag	Sigma-Aldrich	Cat#F7425
Rabbit monoclonal anti-GAPDH (clone D16H11)	Cell Signaling Technology	Cat#5174
Rabbit polyclonal anti-HA tag	Sigma-Aldrich	Cat#H6908
Mouse HDAC1 (clone 10E2)	Santa Cruz Biotech	Cat#sc-81598
IE1/2 (3H4)	Princeton University/Dr. Tom Shenk	N/A
Rabbit monoclonal anti-Myc tag (clone 71D10)	Cell Signaling Technology	Cat#2278
Tubulin (clone DM1A)		Cat#T6199
UL135	Open Biosystems	Custom antibody
Goat anti-mouse secondary antibody (IR Dye 680)	LI-COR Biosciences	Cat#926-68070
Goat anti-rabbit secondary antibody (IR Dye 800)	LI-COR Biosciences	Cat#926-32211

679

680 **RT-qPCR assays**

681 Cells were washed twice in cold PBS and lysed in 400 µl of RNA/DNA lysis buffer
682 (Zymo Research). Total cellular RNA was extracted according to the manufacturer's
683 protocol for Quick-DNA/RNA minipreps. cDNA was synthesized from 1 µg of DNAse-
684 treated RNA using the Vilo cDNA synthesis kit (Invitrogen, Thermo Fisher Scientific).
685 qPCR reactions were prepared with *IDOL* TaqMan assay (ID Hs00982312_m1;
686 ThermoFisher Scientific), Platinum™ Quantitative PCR SuperMix-UDG w/ROX
687 (ThermoFisher Scientific) and 50 ng cDNA. qPCR reactions were run in a QuantStudio

688 3 real time PCR machine (Applied Biosystems). Gene expression was normalized to
689 GAPDH (Hs01922876_u1) or H6PD (Hs00188728_m1) and the ΔΔCT method was
690 used to calculate relative gene expression levels (111, 112). Alternatively, cDNA was
691 quantified using LightCycler SYBR Mix kit (Roche) and corresponding primers to IDOL
692 (BIORAD PrimePCR^{TM} Primers) and H6PD (Forward: 5'-
693 GGACCATTACTTAGGCAAGCA-3' Reverse: 5'-CACGGTCTCTTTCATGATGATCT-3').
694 Assays performed on Light Cycler 480 and corresponding software. Relative expression
695 was determined using the ΔΔCT method normalized to H6PD.

696

697 **Co-immunoprecipitation**

698 Cells were washed twice with PBS and trypsinized. The PBS-washed cell pellet was
699 lysed on ice for 30 minutes in a lysis buffer made of 100 mM Tris/HCl (pH 7.4), 100 mM
700 NaCl, 50 mM NaFI, and 0.5% NP-40. The complete protease inhibitor cocktail (Roche)
701 was added to the lysis buffer according to manufacturer recommendations. Lysates
702 were clarified by centrifugation at 3000 x g for 5 minutes at 4 ^{o}C. A milligram of the
703 lysate was incubated with Pierce anti-myc or anti-HA magnetic beads for 1 h at 4 ^{o}C.
704 The beads were washed 3 times and protein eluted according to manufacturer's
705 protocol.

706

707 **CRISPR/CAS9-mediated knock out of *IDOL***

708 Guide RNAs (gRNAs) used to knock out IDOL were designed using online gRNA design
709 tools at atum.bio and synthego.com. Sequences of the gRNAs are shown in Table 2.

710 The gRNAs were cloned into lentiCRISPR v2 (113). Lentiviruses to deliver the gRNAs
711 were generated by co-transfecting the lentiCRISPR v2 constructs with pDMG.2 and
712 psPAX2 in HEK 293T cells. MRC-5 and THP-1 cells were transduced at a MOI of 3 and
713 10, respectively. Transduced cells were selected with 2 µg/ml puromycin for 2 days.
714 Validation of knock-out was done by blotting for ApoER-2, Sanger sequencing or
715 quantifying levels of IDOL by ELISA. The Synthego gRNA design algorithm
716 (synthego.com) indicates potential off-target genes for the gRNAs and we selected
717 *HDAC1* to evaluate potential off-target effects by western blot analyses.

718 **Table 2. gRNAs used to KO *IDOL* and *luciferase (Luc)* gene (from *Photinus pyralis*)**

Gene	Position	Forward sequence	Reverse sequence
IDOL	16,145,148	CACCG**GCGCCGTGATGATGCAGUAU**[a]	AAACAUACUGCAUCAUCACGGCGCC
IDOL	16,143,526	CACCG**CCUUUUUGUUUUAGGUGUGC**	AAACGUUUCUCAGGUUUAGCCAUAC
IDOL	16,143,613	CACCG**UAUGGCUAAACCUGAGAAAC**	AAACGUUUCUCAGGUUUAGCCAUAC
Luc	1355	CACCG**ACAACUUUACCGACCGCGCC**	AAAC**GGCGCGGUCGGUAAAGUUGU**

719 [a]gRNA sequence is in bold text, and the preceding sequence was used to facilitate cloning onto
720 the lentiCRISPR v2 vector.

721

722 **IDOL ELISA**

723 We used a sandwich ELISA assay (Cusabio) to quantify IDOL protein levels in THP-1
724 cells. Cells were washed in cold PBS and resuspended at 10^8 cells/mL followed by
725 freezing at -20 ^{o}C. Following 3 freeze-thaw cycles, IDOL was quantified according to the

726 manufacturer's protocol. Optical densities were determined using a Clariostar plate
727 reader (BMG Labtech) and sample values were interpolated from a standard curve in
728 GraphPad Prism v9.
729
730 **Cholesterol assay**
731 Fibroblasts were seeded at 3 x 10^5 cells per well in 6-well dishes and incubated
732 overnight. Infections were done at a MOI of 1 for 1 h and the inoculum was removed
733 followed by washing cells twice with PBS. Infected cells were incubated in serum-free
734 media and 50 000 cells were harvested at appropriate time points. Samples were
735 prepared using a cholesterol Glo bioluminescent assay (Promega) according to the
736 manufacturer's instructions. Relative light units were measured using a Clariostar Plus
737 plate reader (BMG Labtech) and sample values were extrapolated from a standard
738 curve in GraphPad Prism v9.
739
740 **Latency assays**
741 Latency assays in CD34+ HPCs were carried out as described previously (58). IDOL expression
742 was induced prior to reactivation by treatment with 1 μM GW3965. Infections for latency in THP-
743 1 cells were done as described previously (52)
744
745 **Acknowledgements**
746 This study was supported by the National Institutes of Allergy and Infectious Diseases/
747 National Institutes of Health (NIAID/NIH) grants AI079059 and AI131598 to FG. KZ was
748 supported by a training grant (T32 AG058503) from the National Institute of Aging. We
749 are grateful for the support of the Flow Cytometry and Human Immune Monitoring

750 Shared Resource, supported through the Cancer Center Support Grant P30 CA023074
751 awarded to University of Arizona. We appreciate technical assistance from Lincoln Gay.
752 We thank Drs. James Alwine (University of Pennsylvania), Lynn Enquist (Princeton
753 University), Jean Wilson (University of Arizona), and John Purdy (University of Arizona)
754 for critical discussions on this work.
755
756

References

1. Goodrum F. 2022. The complex biology of human cytomegalovirus latency and reactivation. *In* M. Kielian TCM, M. J. Roossinck (ed), Advances in Virus Research, 1 ed, vol 112. Academic Press.
2. Goodrum F, Britt W, Mocarski ES. 2022. Cytomegalovirus. *In* Howley PM, Knipe DM, Cohen JL, Damania BA (ed), Fields Virology: DNA Viruses, 7th ed, vol 2. Wolters Kluwer.
3. Hahn G, Jores R, Mocarski ES. 1998. Cytomegalovirus remains latent in a common precursor of dendritic and myeloid cells. Proc Natl Acad Sci U S A 95:3937-42.
4. Min C-K, Shakya AK, Lee B-J, Streblow DN, Caposio P, Yurochko AD. 2020. The Differentiation of Human Cytomegalovirus Infected-Monocytes Is Required for Viral Replication. 10.
5. Reeves MB, MacAry PA, Lehner PJ, Sissons JGP, Sinclair JH. 2005. Latency, chromatin remodeling, and reactivation of human cytomegalovirus in the dendritic cells of healthy carriers. Proceedings of the National Academy of Sciences of the United States of America 102:4140.
6. Reeves MB, Sinclair JH. 2013. Circulating dendritic cells isolated from healthy seropositive donors are sites of human cytomegalovirus reactivation in vivo. J Virol 87:10660-7.
7. Taylor-Wiedeman J, Sissons JGP, Borysiewicz LK, Sinclair JH. 1991. Monocytes are a major site of persistence of human cytomegalovirus in peripheral blood mononuclear cells. 72:2059-2064.
8. Forte E, Swaminathan S, Schroeder MW, Kim JY, Terhune SS, Hummel M. 2018. Tumor Necrosis Factor Alpha Induces Reactivation of Human Cytomegalovirus Independently of Myeloid Cell Differentiation following Posttranscriptional Establishment of Latency. mBio 9:e01560-18.
9. Söderberg-Nauclér C, Fish KN, Nelson JA. 1997. Reactivation of Latent Human Cytomegalovirus by Allogeneic Stimulation of Blood Cells from Healthy Donors. Cell 91:119-126.
10. Reeves MB, Compton T. 2011. Inhibition of inflammatory interleukin-6 activity via extracellular signal-regulated kinase-mitogen-activated protein kinase signaling antagonizes human cytomegalovirus reactivation from dendritic cells. J Virol 85:12750-8.
11. Buehler J, Zeltzer S, Reitsma J, Petrucelli A, Umashankar M, Rak M, Zagallo P, Schroeder J, Terhune S, Goodrum F. 2016. Opposing Regulation of the EGF Receptor: A Molecular Switch Controlling Cytomegalovirus Latency and Replication. PLOS Pathogens 12:e1005655.
12. Weekes MP, Tan SYL, Poole E, Talbot S, Antrobus R, Smith DL, Montag C, Gygi SP, Sinclair JH, Lehner PJ. 2013. Latency-Associated Degradation of the MRP1 Drug Transporter During Latent Human Cytomegalovirus Infection. Science 340:199.
13. Le VTK, Trilling M, Hengel H. 2011. The Cytomegaloviral Protein pUL138 Acts as Potentiator of Tumor Necrosis Factor (TNF) Receptor 1 Surface Density To Enhance ULb'-Encoded Modulation of TNF-α Signaling. Journal of Virology 85:13260.
14. Montag C, Wagner JA, Gruska I, Vetter B, Wiebusch L, Hagemeier C. 2011. The Latency-Associated UL138 Gene Product of Human Cytomegalovirus Sensitizes Cells to Tumor Necrosis Factor Alpha (TNF-α) Signaling by Upregulating TNF-α Receptor 1 Cell Surface Expression. 85:11409-11421.
15. Albright ER, Mickelson CK, Kalejta RF. 2021. Human Cytomegalovirus UL138 Protein Inhibits the STING Pathway and Reduces Interferon Beta mRNA Accumulation during Lytic and Latent Infections. mBio 12:e0226721-e0226721.
16. Zarrella K, Longmire P, Zeltzer S, Collins-McMillen D, Hancock M, Buehler J, Reitsma JM, Terhune SS, Nelson JA, Goodrum F. 2023. Human Cytomegalovirus UL138 Interaction with USP1 Activates STAT1 in infection. bioRxiv doi:10.1101/2023.02.07.527452.
17. Lee SH, Albright ER, Lee J-H, Jacobs D, Kalejta RF. 2015. Cellular defense against latent colonization foiled by human cytomegalovirus UL138 protein. Science advances 1:e1501164-e1501164.

804 18. Umashankar M, Rak M, Bughio F, Zagallo P, Caviness K, Goodrum FD. 2014. Antagonistic
805 Determinants Controlling Replicative and Latent States of Human Cytomegalovirus Infection.
806 Journal of Virology 88:5987.
807 19. Rak MA, Buehler J, Zeltzer S, Reitsma J, Molina B, Terhune S, Goodrum F. 2018. Human
808 Cytomegalovirus UL135 Interacts with Host Adaptor Proteins To Regulate Epidermal Growth
809 Factor Receptor and Reactivation from Latency. 92:e00919-18.
810 20. Buehler J, Carpenter E, Zeltzer S, Igarashi S, Rak M, Mikell I, Nelson JA, Goodrum F. 2019. Host
811 signaling and EGR1 transcriptional control of human cytomegalovirus replication and latency.
812 PLOS Pathogens 15:e1008037.
813 21. Caviness K, Bughio F, Crawford LB, Streblow DN, Nelson JA, Caposio P, Goodrum F. 2016.
814 Complex Interplay of the UL136 Isoforms Balances Cytomegalovirus
815 Replication and Latency. mBio 7:e01986-15.
816 22. Caviness K, Cicchini L, Rak M, Umashankar M, Goodrum F. 2014. Complex expression of the
817 UL136 gene of human cytomegalovirus results in multiple protein isoforms with unique roles in
818 replication. J Virol 88:14412-25.
819 23. Mikell I, Crawford LB, Hancock MH, Mitchell J, Buehler J, Goodrum F, Nelson JA. 2019. HCMV
820 miR-US22 down-regulation of EGR-1 regulates CD34+ hematopoietic progenitor cell
821 proliferation and viral reactivation. PLoS Pathog 15:e1007854.
822 24. Min IM, Pietramaggiori G, Kim FS, Passegué E, Stevenson KE, Wagers AJ. 2008. The Transcription
823 Factor EGR1 Controls Both the Proliferation and Localization of Hematopoietic Stem Cells. Cell
824 Stem Cell 2:380-391.
825 25. Collins-McMillen D, Kamil J, Moorman N, Goodrum F. 2020. Control of Immediate Early Gene
826 Expression for Human Cytomegalovirus Reactivation. Front Cell Infect Microbiol 10:476.
827 26. Krishna BA, Wass AB, O'Connor CM. 2020. Activator protein-1 transactivation of the major
828 immediate early locus is a determinant of cytomegalovirus reactivation from latency. Proc Natl
829 Acad Sci U S A 117:20860-20867.
830 27. Hale AE, Collins-McMillen D, Lenarcic EM, Igarashi S, Kamil JP, Goodrum F, Moorman NJ. 2020.
831 FOXO transcription factors activate alternative major immediate early promoters to induce
832 human cytomegalovirus reactivation. Proc Natl Acad Sci U S A 117:18764-18770.
833 28. Kew VG, Yuan J, Meier J, Reeves MB. 2014. Mitogen and stress activated kinases act co-
834 operatively with CREB during the induction of human cytomegalovirus immediate-early gene
835 expression from latency. PLoS Pathog 10:e1004195.
836 29. Crawford LB, Kim JH, Collins-McMillen D, Lee BJ, Landais I, Held C, Nelson JA, Yurochko AD,
837 Caposio P. 2018. Human Cytomegalovirus Encodes a Novel FLT3 Receptor Ligand Necessary for
838 Hematopoietic Cell Differentiation and Viral Reactivation. MBio 9.
839 30. Hancock MH, Crawford LB, Perez W, Struthers HM, Mitchell J, Caposio P. 2021. Human
840 Cytomegalovirus UL7, miR-US5-1, and miR-UL112-3p Inactivation of FOXO3a Protects CD34(+)
841 Hematopoietic Progenitor Cells from Apoptosis. mSphere 6.
842 31. Scotti E, Hong C, Yoshinaga Y, Tu Y, Hu Y, Zelcer N, Boyadjian R, de Jong PJ, Young SG, Fong LG,
843 Tontonoz P. 2011. Targeted disruption of the idol gene alters cellular regulation of the low-
844 density lipoprotein receptor by sterols and liver x receptor agonists. Molecular and cellular
845 biology 31:1885-1893.
846 32. de Bruin RG, Shiue L, Prins J, de Boer HC, Singh A, Fagg WS, van Gils JM, Duijs JMGJ, Katzman S,
847 Kraaijeveld AO, Böhringer S, Leung WY, Kielbasa SM, Donahue JP, van der Zande PHJ, Sijbom R,
848 van Alem CMA, Bot I, van Kooten C, Jukema JW, Van Esch H, Rabelink TJ, Kazan H, Biessen EAL,
849 Ares Jr M, van Zonneveld AJ, van der Veer EP. 2016. Quaking promotes monocyte differentiation
850 into pro-atherogenic macrophages by controlling pre-mRNA splicing and gene expression.
851 Nature Communications 7:10846.

852 33. Liu Y, Tingart M, Lecouturier S, Li J, Eschweiler J. 2021. Identification of co-expression network
853 correlated with different periods of adipogenic and osteogenic differentiation of BMSCs by
854 weighted gene co-expression network analysis (WGCNA). BMC Genomics 22:254.
855 34. Scotti E, Calamai M, Goulbourne CN, Zhang L, Hong C, Lin RR, Choi J, Pilch PF, Fong LG, Zou P,
856 Ting AY, Pavone FS, Young SG, Tontonoz P. 2013. IDOL stimulates clathrin-independent
857 endocytosis and multivesicular body-mediated lysosomal degradation of the low-density
858 lipoprotein receptor. Molecular and cellular biology 33:1503-1514.
859 35. Hong C, Duit S, Jalonen P, Out R, Scheer L, Sorrentino V, Boyadjian R, Rodenburg KW, Foley E,
860 Korhonen L, Lindholm D, Nimpf J, van Berkel TJC, Tontonoz P, Zelcer N. 2010. The E3 ubiquitin
861 ligase IDOL induces the degradation of the low density lipoprotein receptor family members
862 VLDLR and ApoER2. The Journal of biological chemistry 285:19720-19726.
863 36. Zelcer N, Hong C, Boyadjian R, Tontonoz P. 2009. LXR regulates cholesterol uptake through Idol-
864 dependent ubiquitination of the LDL receptor. Science 325:100-4.
865 37. Moy MA, Collins-McMillen D, Crawford L, Parkins C, Zeltzer S, Caviness K, Capozio P, Goodrum F.
866 2023. UL135 and UL136 Epistasis Controls Reactivation of Human Cytomegalovirus. In revision,
867 Journal of Virology BIORXIV/2023/525282.
868 38. Glickman MH, Ciechanover A. 2002. The ubiquitin-proteasome proteolytic pathway: destruction
869 for the sake of construction. Physiol Rev 82:373-428.
870 39. Pickart CM. 2004. Back to the future with ubiquitin. Cell 116:181-90.
871 40. Zhang J, Liu Q. 2015. Cholesterol metabolism and homeostasis in the brain. Protein & cell 6:254-
872 264.
873 41. Zhang L, Reue K, Fong LG, Young SG, Tontonoz P. 2012. Feedback regulation of cholesterol
874 uptake by the LXR-IDOL-LDLR axis. Arteriosclerosis, thrombosis, and vascular biology 32:2541-
875 2546.
876 42. Gao J, Marosi M, Choi J, Achiro JM, Kim S, Li S, Otis K, Martin KC, Portera-Cailliau C, Tontonoz P.
877 2017. The E3 ubiquitin ligase IDOL regulates synaptic ApoER2 levels and is important for
878 plasticity and learning. eLife 6:e29178.
879 43. Nelson JK, Cook ECL, Loregger A, Hoeksema MA, Scheij S, Kovacevic I, Hordijk PL, Ovaa H, Zelcer
880 N. 2016. Deubiquitylase Inhibition Reveals Liver X Receptor-independent Transcriptional
881 Regulation of the E3 Ubiquitin Ligase IDOL and Lipoprotein Uptake. The Journal of biological
882 chemistry 291:4813-4825.
883 44. Anonymous. 2004. Cytomegalovirus. Am J Transplant 4 Suppl 10:51-8.
884 45. Du Y, Zhang G, Liu Z. 2018. Human cytomegalovirus infection and coronary heart disease: a
885 systematic review. Virology journal 15:31-31.
886 46. Gudleski-O'Regan N, Greco TM, Cristea IM, Shenk T. 2012. Increased expression of LDL receptor-
887 related protein 1 during human cytomegalovirus infection reduces virion cholesterol and
888 infectivity. Cell Host Microbe 12:86-96.
889 47. Xi Y, Harwood S, Wise LM, Purdy JG. 2019. Human Cytomegalovirus pUL37x1 Is Important for
890 Remodeling of Host Lipid Metabolism. J Virol 93.
891 48. Xi Y, Lindenmayer L, Kline I, von Einem J, Purdy JG. 2021. Human Cytomegalovirus Uses a Host
892 Stress Response To Balance the Elongation of Saturated/Monounsaturated and Polyunsaturated
893 Very-Long-Chain Fatty Acids. mBio 12.
894 49. Yu Y, Maguire TG, Alwine JC. 2012. Human cytomegalovirus infection induces adipocyte-like
895 lipogenesis through activation of sterol regulatory element binding protein 1. J Virol 86:2942-9.
896 50. Yu Y, Pierciey FJ, Jr., Maguire TG, Alwine JC. 2013. PKR-like endoplasmic reticulum kinase is
897 necessary for lipogenic activation during HCMV infection. PLoS Pathog 9:e1003266.

898 51. Collins-McMillen D, Rak M, Buehler JC, Igarashi-Hayes S, Kamil JP, Moorman NJ, Goodrum F.
899 2019. Alternative promoters drive human cytomegalovirus reactivation from latency. Proc Natl
900 Acad Sci U S A 116:17492-17497.
901 52. Collins-McMillen D, Rak M, Buehler JC, Igarashi-Hayes S, Kamil JP, Moorman NJ, Goodrum F.
902 2019. Alternative promoters drive human cytomegalovirus reactivation from latency.
903 Proceedings of the National Academy of Sciences 116:17492.
904 53. Arcangeletti M-C, Vasile Simone R, Rodighiero I, De Conto F, Medici M-C, Maccari C, Chezzi C,
905 Calderaro A. 2016. Human cytomegalovirus reactivation from latency: validation of a "switch"
906 model in vitro. Virology journal 13:179-179.
907 54. Yee L-F, Lin PL, Stinski MF. 2007. Ectopic expression of HCMV IE72 and IE86 proteins is sufficient
908 to induce early gene expression but not production of infectious virus in undifferentiated
909 promonocytic THP-1 cells. Virology 363:174-188.
910 55. Weinshenker BG, Wilton S, Rice GP. 1988. Phorbol ester-induced differentiation permits
911 productive human cytomegalovirus infection in a monocytic cell line. J Immunol 140:1625-31.
912 56. Wagenknecht N, Reuter N, Scherer M, Reichel A, Muller R, Stamminger T. 2015. Contribution of
913 the Major ND10 Proteins PML, hDaxx and Sp100 to the Regulation of Human Cytomegalovirus
914 Latency and Lytic Replication in the Monocytic Cell Line THP-1. Viruses 7:2884-907.
915 57. Lee CH, Lee GC, Chan YJ, Chiou CJ, Ahn JH, Hayward GS. 1999. Factors affecting human
916 cytomegalovirus gene expression in human monocyte cell lines. Mol Cells 9:37-44.
917 58. Peppenelli M, Buehler J, Goodrum F. 2021. Human Hematopoietic Long-Term Culture (hLTC) for
918 Human Cytomegalovirus Latency and Reactivation. Methods Mol Biol 2244:83-101.
919 59. Ramirez RN, El-Ali NC, Mager MA, Wyman D, Conesa A, Mortazavi A. 2017. Dynamic Gene
920 Regulatory Networks of Human Myeloid Differentiation. Cell Syst 4:416-429.e3.
921 60. Martinez FO, Gordon S, Locati M, Mantovani A. 2006. Transcriptional Profiling of the Human
922 Monocyte-to-Macrophage Differentiation and Polarization: New Molecules and Patterns of
923 Gene Expression. The Journal of Immunology 177:7303.
924 61. Fagerberg B, Gnarpe J, Gnarpe H, Agewall S, Wikstrand J. 1999. Chlamydia pneumoniae but not
925 cytomegalovirus antibodies are associated with future risk of stroke and cardiovascular disease:
926 a prospective study in middle-aged to elderly men with treated hypertension. Stroke 30:299-
927 305.
928 62. Pizzorno MC, Hayward GS. 1990. The IE2 gene products of human cytomegalovirus specifically
929 down-regulate expression from the major immediate-early promoter through a target located
930 near the cap site. J Virol 64:6154-6165.
931 63. Cherrington JM, Khoury EL, Mocarski ES. 1991. Human cytomegalovirus ie2 negatively regulates
932 alpha gene expression via a short target sequence near the transcription start site. J Virol
933 65:887-96.
934 64. Liu B, Hermiston TW, Stinski MF. 1991. A cis-acting element in the major immediate early (IE)
935 promoter of human cytomegalovirus is required for negative regulation by IE2. J Virol 65:897-
936 903.
937 65. Macias MP, Stinski MF. 1993. An in vitro system for human cytomegalovirus immediate early 2
938 protein (IE2)-mediated site-dependent repression of transcription and direct binding of IE2 to
939 the major immediate early promoter. Proc Natl Acad Sci U S A 90:707-11.
940 66. Caviness K, Bughio F, Crawford LB, Streblow DN, Nelson JA, Caposio P, Goodrum F. 2016.
941 Complex Interplay of the UL136 Isoforms Balances Cytomegalovirus Replication and Latency.
942 mBio 7:e01986.
943 67. Lee SD, Tontonoz P. 2015. Liver X receptors at the intersection of lipid metabolism and
944 atherogenesis. Atherosclerosis 242:29-36.

945 68. Janowski BA, Grogan MJ, Jones SA, Wisely GB, Kliewer SA, Corey EJ, Mangelsdorf DJ. 1999.
946 Structural requirements of ligands for the oxysterol liver X receptors LXRalpha and LXRbeta. Proc
947 Natl Acad Sci U S A 96:266-71.
948 69. Janowski BA, Willy PJ, Devi TR, Falck JR, Mangelsdorf DJ. 1996. An oxysterol signalling pathway
949 mediated by the nuclear receptor LXRα. Nature 383:728-731.
950 70. Peet DJ, Janowski BA, Mangelsdorf DJ. 1998. The LXRs: a new class of oxysterol receptors.
951 Current Opinion in Genetics & Development 8:571-575.
952 71. Fagerberg L, Hallström BM, Oksvold P, Kampf C, Djureinovic D, Odeberg J, Habuka M,
953 Tahmasebpoor S, Danielsson A, Edlund K, Asplund A, Sjöstedt E, Lundberg E, Szigyarto CA, Skogs
954 M, Takanen JO, Berling H, Tegel H, Mulder J, Nilsson P, Schwenk JM, Lindskog C, Danielsson F,
955 Mardinoglu A, Sivertsson A, von Feilitzen K, Forsberg M, Zwahlen M, Olsson I, Navani S, Huss M,
956 Nielsen J, Ponten F, Uhlén M. 2014. Analysis of the human tissue-specific expression by genome-
957 wide integration of transcriptomics and antibody-based proteomics. Mol Cell Proteomics
958 13:397-406.
959 72. Fernandez-Ruiz I, Puchalska P, Narasimhulu CA, Sengupta B, Parthasarathy S. 2016. Differential
960 lipid metabolism in monocytes and macrophages: influence of cholesterol loading[S]. Journal of
961 Lipid Research 57:574-586.
962 73. Cimato TR, Palka BA, Lang JK, Young RF. 2013. LDL Cholesterol Modulates Human CD34+ HSPCs
963 through Effects on Proliferation and the IL-17 G-CSF Axis. PLOS ONE 8:e73861.
964 74. Morgan PK, Fang L, Lancaster GI, Murphy AJ. 2020. Hematopoiesis is regulated by cholesterol
965 efflux pathways and lipid rafts: connections with cardiovascular diseases: Thematic Review
966 Series: Biology of Lipid Rafts. Journal of Lipid Research 61:667-675.
967 75. Soehnlein O, Swirski FK. 2013. Hypercholesterolemia links hematopoiesis with atherosclerosis.
968 Trends Endocrinol Metab 24:129-36.
969 76. Radley JM, Ellis S, Palatsides M, Williams B, Bertoncello I. 1999. Ultrastructure of primitive
970 hematopoietic stem cells isolated using probes of functional status. Exp Hematol 27:365-9.
971 77. Shariatmadar S, Sharma S, Cabana R, Powell S, Ruiz P, Krishan A. 2008. Electronic volume of
972 CD34 positive cells from peripheral blood apheresis samples. Cytometry B Clin Cytom 74:182-8.
973 78. Vacanti MP, Roy A, Cortiella J, Bonassar L, Vacanti CA. 2001. Identification and initial
974 characterization of spore-like cells in adult mammals. J Cell Biochem 80:455-60.
975 79. Calkin AC, Goult BT, Zhang L, Fairall L, Hong C, Schwabe JWR, Tontonoz P. 2011. FERM-
976 dependent E3 ligase recognition is a conserved mechanism for targeted degradation of
977 lipoprotein receptors. 108:20107-20112.
978 80. Liu B, Ma Y, Huang Y, Liu Z, Ruan Q, Qi Y. 2022. Inhibition of Human Cytomegalovirus Particle
979 Maturation by Activation of Liver X Receptor. Frontiers in microbiology 13:846386-846386.
980 81. Wang Q, Ma X, Chen Y, Zhang L, Jiang M, Li X, Xiang R, Miao R, Hajjar David P, Duan Y, Han J.
981 2014. Identification of interferon-γ as a new molecular target of liver X receptor. Biochemical
982 Journal 459:345-354.
983 82. Sainz B, LaMarca HL, Garry RF, Morris CA. 2005. Synergistic inhibition of human cytomegalovirus
984 replication by interferon-alpha/beta and interferon-gamma. Virology Journal 2:14.
985 83. Kropp KA, Robertson KA, Sing G, Rodriguez-Martin S, Blanc M, Lacaze P, Hassim MFBN,
986 Khondoker MR, Busche A, Dickinson P, Forster T, Strobl B, Mueller M, Jonjic S, Angulo A, Ghazal
987 P. 2011. Reversible inhibition of murine cytomegalovirus replication by gamma interferon (IFN-
988 γ) in primary macrophages involves a primed type I IFN-signaling subnetwork for full
989 establishment of an immediate-early antiviral state. Journal of virology 85:10286-10299.
990 84. Wang Y, Li G-L, Qi Y-L, Li L-Y, Wang L-F, Wang C-R, Niu X-R, Liu T-X, Wang J, Yang G-Y, Zeng L, Chu
991 B-B. 2022. Pseudorabies Virus Inhibits Expression of Liver X Receptors to Assist Viral Infection.
992 Viruses 14:514.

993 85. Lange PT, Schorl C, Sahoo D, Tarakanova VL. 2018. Liver X Receptors Suppress Activity of
994 Cholesterol and Fatty Acid Synthesis Pathways To Oppose Gammaherpesvirus Replication. mBio
995 9:e01115-18.
996 86. Lange PT, Jondle CN, Darrah EJ, Johnson KE, Tarakanova VL. 2019. LXR Alpha Restricts
997 Gammaherpesvirus Reactivation from Latently Infected Peritoneal Cells. Journal of virology
998 93:e02071-18.
999 87. Zeng J, Wu Y, Liao Q, Li L, Chen X, Chen X. 2012. Liver X receptors agonists impede hepatitis C
1000 virus infection in an Idol-dependent manner. Antiviral Res 95:245-56.
1001 88. Bocchetta S, Maillard P, Yamamoto M, Gondeau C, Douam F, Lebreton S, Lagaye S, Pol S, Helle F,
1002 Plengpanich W, Guerin M, Bourgine M, Michel ML, Lavillette D, Roingeard P, le Goff W,
1003 Budkowska A. 2014. Up-regulation of the ATP-binding cassette transporter A1 inhibits hepatitis
1004 C virus infection. PLoS One 9:e92140.
1005 89. Jiang H, Badralmaa Y, Yang J, Lempicki R, Hazen A, Natarajan V. 2012. Retinoic acid and liver X
1006 receptor agonist synergistically inhibit HIV infection in CD4+ T cells by up-regulating ABCA1-
1007 mediated cholesterol efflux. Lipids Health Dis 11:69.
1008 90. Dubrovsky L, Van Duyne R, Senina S, Guendel I, Pushkarsky T, Sviridov D, Kashanchi F, Bukrinsky
1009 M. 2012. Liver X receptor agonist inhibits HIV-1 replication and prevents HIV-induced reduction
1010 of plasma HDL in humanized mouse model of HIV infection. Biochem Biophys Res Commun
1011 419:95-8.
1012 91. Hanley TM, Viglianti GA. 2011. Nuclear receptor signaling inhibits HIV-1 replication in
1013 macrophages through multiple trans-repression mechanisms. J Virol 85:10834-50.
1014 92. Sheng XX, Sun YJ, Zhan Y, Qu YR, Wang HX, Luo M, Liao Y, Qiu XS, Ding C, Fan HJ, Mao X. 2016.
1015 The LXR ligand GW3965 inhibits Newcastle disease virus infection by affecting cholesterol
1016 homeostasis. Arch Virol 161:2491-501.
1017 93. Zeng J, Wu Y, Liao Q, Li L, Chen X, Chen X. 2012. Liver X receptors agonists impede hepatitis C
1018 virus infection in an Idol-dependent manner. Antiviral Research 95:245-256.
1019 94. Syed GH, Tang H, Khan M, Hassanein T, Liu J, Siddiqui A. 2014. Hepatitis C virus stimulates low-
1020 density lipoprotein receptor expression to facilitate viral propagation. Journal of virology
1021 88:2519-2529.
1022 95. Albecka A, Belouzard S, Op de Beeck A, Descamps V, Goueslain L, Bertrand-Michel J, Tercé F,
1023 Duverlie G, Rouillé Y, Dubuisson J. 2012. Role of low-density lipoprotein receptor in the hepatitis
1024 C virus life cycle. Hepatology 55:998-1007.
1025 96. Molina S, Castet V, Fournier-Wirth C, Pichard-Garcia L, Avner R, Harats D, Roitelman J, Barbaras
1026 R, Graber P, Ghersa P, Smolarsky M, Funaro A, Malavasi F, Larrey D, Coste J, Fabre JM, Sa-Cunha
1027 A, Maurel P. 2007. The low-density lipoprotein receptor plays a role in the infection of primary
1028 human hepatocytes by hepatitis C virus. J Hepatol 46:411-9.
1029 97. Sun B, Yang X, Hou F, Yu X, Wang Q, Oh HS, Raja P, Pesola JM, Vanni EAH, McCarron S, Morris-
1030 Love J, Ng AHM, Church GM, Knipe DM, Coen DM, Pan D. 2021. Regulation of host and virus
1031 genes by neuronal miR-138 favours herpes simplex virus 1 latency. Nat Microbiol 6:682-696.
1032 98. Pan D, Flores O, Umbach JL, Pesola JM, Bentley P, Rosato PC, Leib DA, Cullen BR, Coen DM.
1033 2014. A neuron-specific host microRNA targets herpes simplex virus-1 ICP0 expression and
1034 promotes latency. Cell Host Microbe 15:446-56.
1035 99. Liu X, Acharya D, Krawczyk E, Kangas C, Gack MU, He B. 2021. Herpesvirus-mediated
1036 stabilization of ICP0 expression neutralizes restriction by TRIM23. Proc Natl Acad Sci U S A 118.
1037 100. Chang TH, Wang SS, Chen LW, Shih YJ, Chang LK, Liu ST, Chang PJ. 2016. Regulation of the
1038 Abundance of Kaposi's Sarcoma-Associated Herpesvirus ORF50 Protein by Oncoprotein MDM2.
1039 PLoS Pathog 12:e1005918.

1040 101. Chmura JC, Herold K, Ruffin A, Atuobi T, Fabiyi Y, Mitchell AE, Choi YB, Ehrlich ES. 2017. The Itch
1041 ubiquitin ligase is required for KSHV RTA induced vFLIP degradation. Virology 501:119-126.
1042 102. Ehrlich ES, Chmura JC, Smith JC, Kalu NN, Hayward GS. 2014. KSHV RTA abolishes NFkappaB
1043 responsive gene expression during lytic reactivation by targeting vFLIP for degradation via the
1044 proteasome. PLoS One 9:e91359.
1045 103. Gandon S. 2016. Why Be Temperate: Lessons from Bacteriophage λ. Trends in Microbiology
1046 24:356-365.
1047 104. Atsumi S, Little JW. 2006. Role of the lytic repressor in prophage induction of phage lambda as
1048 analyzed by a module-replacement approach. Proceedings of the National Academy of Sciences
1049 of the United States of America 103:4558-4563.
1050 105. Schubert RA, Dodd IB, Egan JB, Shearwin KE. 2007. Cro's role in the CI Cro bistable switch is
1051 critical for {lambda}'s transition from lysogeny to lytic development. Genes & development
1052 21:2461-2472.
1053 106. Cortes MG, Trinh JT, Zeng L, Balazsi G. 2017. Late-Arriving Signals Contribute Less to Cell-Fate
1054 Decisions. Biophys J 113:2110-2120.
1055 107. Kobiler O, Rokney A, Oppenheim AB. 2007. Phage lambda CIII: a protease inhibitor regulating
1056 the lysis-lysogeny decision. PLoS One 2:e363.
1057 108. Little JW, Shepley DP, Wert DWJTEj. 1999. Robustness of a gene regulatory circuit. 18:4299-
1058 4307.
1059 109. Hernandez-Doria JD, Sperandio V. 2018. Bacteriophage Transcription Factor Cro Regulates
1060 Virulence Gene Expression in Enterohemorrhagic Escherichia coli. Cell Host & Microbe 23:607-
1061 617.e6.
1062 110. Umashankar M, Petrucelli A, Cicchini L, Caposio P, Kreklywich CN, Rak M, Bughio F, Goldman DC,
1063 Hamlin KL, Nelson JA, Fleming WH, Streblow DN, Goodrum F. 2011. A Novel Human
1064 Cytomegalovirus Locus Modulates Cell Type-Specific Outcomes of Infection. PLOS Pathogens
1065 7:e1002444.
1066 111. Rao X, Huang X, Zhou Z, Lin X. 2013. An improvement of the 2^(-delta delta CT) method for
1067 quantitative real-time polymerase chain reaction data analysis. Biostat Bioinforma Biomath
1068 3:71-85.
1069 112. Winer J, Jung CK, Shackel I, Williams PM. 1999. Development and validation of real-time
1070 quantitative reverse transcriptase-polymerase chain reaction for monitoring gene expression in
1071 cardiac myocytes in vitro. Anal Biochem 270:41-9.
1072 113. Sanjana NE, Shalem O, Zhang F. 2014. Improved vectors and genome-wide libraries for CRISPR
1073 screening. Nat Methods 11:783-784.

1074

1075

1076 ## Figure legends

1077

1078 **Figure 1. UL136p33 isoform is rapidly turned over by the proteasome.** (A)
1079 Schematic depiction of the *UL133-UL138* polycistronic gene locus and UL136 protein
1080 isoforms. A C-terminal myc tag is used to detect UL136 isoforms. Red lines represent
1081 lysine residues, and the black box shows the putative transmembrane domain. (B-D)

1082 Fibroblasts were infected with TB40/E-*UL136*$_{myc}$ virus at a MOI of 1. (B) At 48 hpi, cells
1083 were treated with 50 µg/ml cycloheximide (CHX) for 6 h. Alternatively, mock- or TB40/E-
1084 infected cells were treated with CHX in the context of proteasomal (MG132) or
1085 lysosomal (NH_4Cl) inhibition (right panel). UL136$_{myc}$ protein isoforms or tubulin as a
1086 loading control were detected by immunoblotting using by a monoclonal α-myc antibody
1087 or tubulin, respectively (left panel). (C) Cells were untreated or treated with CHX at 48
1088 hpi and UL136 decay was analyzed over a 6-hour time course by immunoblotting. (D)
1089 Relative quantification of UL136 isoforms normalized to tubulin. HPT, hours post
1090 treatment
1091

1092 **Figure 2. Stabilizing UL136p33 results in virus that fails to establish latency.** (A)
1093 Fibroblasts were transduced with lentiviruses engineered to express p33$_{myc}$ or p33$_{K\rightarrow R}$
1094 and protein decay was analyzed by immunoblotting following CHX treatment. (B)
1095 Fibroblasts were infected with TB40/E-*UL136*$_{myc}$ or -*UL136*$_{myc}$*ΔK→R* viruses (MOI =1)
1096 and treated with CHX at 48 hpi or left untreated. Protein decay was analyzed as
1097 described in Figure 1C. (C) Fibroblasts were infected at a MOI of 0.02 and samples
1098 collected for $TCID_{50}$ at indicated times. All data points are an average of 3 biological
1099 replicates and error bars represent standard deviation. (D) CD34+ HPCs were infected
1100 with *UL136*$_{myc}$ or *UL136*$_{myc}$*ΔK→R* viruses (MOI=2). Infected cells were purified by FACS
1101 at 1 dpi seeded into long term culture. At 10 days, half of the culture was reactivated by
1102 seeding intact cells by limiting dilution into co-culture with fibroblasts in a cytokine-rich
1103 media to promote myeloid differentiation (reactivation). The other half of the culture was
1104 mechanically lysed and seeded onto fibroblasts as the pre-reactivation control. The

1105 frequency of infectious centers was determined for each sample by extreme limiting
1106 dilution. (C-D) The data represents replicates with cells from 3 independent donors. The
1107 means were compared with two-way analysis of variance (ANOVA) with a Tukey post
1108 hoc test and the were no significant differences. **, $p<0.01$; ***, $p<0.001$.

1109

1110 **Figure 3. The host E3 ligase IDOL specifically targets UL136p33 for turnover.** (A)
1111 HEK cells were transiently transfected with plasmids expressing UL136p33, IDOL,
1112 empty vector, or the indicated combinations. UL136p33 or IDOL was
1113 immunoprecipitated from protein lysates using α-myc or α-HA magnetic beads. Protein
1114 was detected by immunoblotting using the antibodies indicated. Lysates were blotted as
1115 a control for expression and GAPDH used as a loading control. (B) HEK cells were
1116 transiently transfected with plasmids expressing $p33_{\Delta K \rightarrow R}$, IDOL, or empty vector.
1117 Proteins were detected by immunoblotting using α-myc or α-HA monoclonal antibodies.
1118 (C) Protein densities of UL136p33 (from panel A) or $p33_{\Delta K \rightarrow R}$ (from panel B) relative to
1119 their loading control. (D) HEK cells were transiently transfected to express UL136p33 or
1120 $p33_{\Delta K \rightarrow R.}$ IDOL was induced 48 hours later with 2 μM of LXR-agonists, GW3965 or
1121 HBX41-108, or vehicle (DMSO) for 6 h. Detection of ApoER-2 was used as a proxy for
1122 validating the induction of IDOL. $p33_{myc}$, $p33_{K \rightarrow R}$, and tubulin as a loading control were
1123 detected by immunoblotting using α-myc or α-tubulin. (E-G) HEK 293T cells were
1124 transfected with plasmids expressing (E) IDOL, p25 or empty vector or (F) IDOL, p23 or
1125 empty vector. Proteins detected by immunoblotting using antibodies to FLAG or HA to
1126 detect the indicated proteins. Tubulin or GAPDH were used as loading controls for
1127 normalization. (G) Relative p25 or p23 densities. (H) HEK 293T cells were co-

1128 transfected with plasmids expressing UL136p33, the E3 ligase Cbl or empty vector.
1129 Proteins were detected by immunoblotting using antibodies to the myc epitope tag or
1130 cbl. (I) Relative UL136p33 densities were measured and quantified. All data points
1131 represent the mean of at least 3 independent replicates and the means were compared
1132 by two-way ANOVA with a Tukey post hoc test. Error bars represent standard deviation.
1133 ns, non-significant $p>0.05$; ****, $p<0.0001$.
1134

1135 **Figure 4. IDOL expression in HCMV-infected fibroblasts impacts UL136p33**
1136 **stability.** (A) Fibroblasts were mock-infected or infected with *UL136*$_{myc}$ or
1137 *UL136*$_{myc}$*ΔK→R* viruses at a MOI of 1 and total RNA extracted at indicated time points.
1138 RT-qPCR was used to quantify relative *IDOL* transcripts using the ΔΔCT method. *IDOL*
1139 transcripts were normalized to GAPDH and compared to expression levels in mock
1140 samples at 1 dpi. (B) Fibroblasts were infected with TB40/E at a MOI of 1 followed by
1141 incubation in serum-free media. Cholesterol concentrations were measured and
1142 compared to mock-infected cells at 1 dpi. (C) Fibroblasts were mock-infected or infected
1143 with *UL136*$_{myc}$ or *UL136*$_{myc}$*ΔK→R* viruses at a MOI of 1. At 2 dpi, IDOL expression was
1144 induced by treatment with 2 μM GW3965 or HBX41-108 for 6 h followed by western blot
1145 evaluation of UL136p33 levels (left). Relative UL136p33 levels are quantified in (D). (E)
1146 *IDOL* KO cell lysates were analyzed by western blot to evaluate ApoER-2 expression
1147 levels compared to a *Luc* KO control. To evaluate CRISPR/CAS9 off-target effects we
1148 measured HDAC1 in *Luc* or *IDOL* KO cell lysates. (F) *UL136*$_{myc}$ or *UL136*$_{myc}$*ΔK→R*
1149 viruses were used to infect either *Luc* or *IDOL* KO cells at a MOI of 1. Cell lysates were
1150 collected at indicated times and evaluated for UL136p33. IE1 and IE2 protein levels that

1151 are quantified in panels G and H. (G) Quantification p33 protein densities relative to the
1152 Luc KO at 2 dpi in each infection condition, *UL136*$_{myc}$ and *UL136*$_{myc}$Δ*K→R*. (H)
1153 Quantification of IE2 protein densities relative to *Luc* KO at 2 dpi in each infection
1154 condition, *UL136*$_{myc}$ and *UL136*$_{myc}$Δ*K→R*. Quantitative data points represent the mean
1155 of 3 independent replicates and error bars represent standard deviation. Differences in
1156 the means were compared using two-way ANOVA with a Tukey post hoc test. ns,
1157 p>0.05; *, p<0.05; **, p<0.01; ***, p<0.001; ****, p<0.0001.

1158

1159 **Figure 5. IDOL impacts viral protein expression in a THP-1 cell latency model.** (A)
1160 Total RNA was extracted from mock-, *UL136*$_{myc}$- or *UL136*$_{myc}$*ΔK→R*-infected THP-1
1161 cells at indicated time points. At 5 dpi, cells were treated with TPA to induce
1162 differentiation or the vehicle control (DMSO). cDNA was synthesized from the RNA and
1163 qPCR was used to determine the relative expression levels of *IDOL* transcripts
1164 compared to the low copy cellular housekeeping gene *H6PD* using the ΔΔCT method.
1165 (B) Validation of *IDOL* KO in undifferentiated THP-1 cells was confirmed by ELISA.
1166 Where indicated, cells were treated with TPA as a positive control for the loss of IDOL.
1167 (C) Immunoblot of HDAC1 in *Luc* control or *IDOL* KO THP-1 cells to rule out off-target
1168 CRISPR/CAS9 effects. (D) *IDOL* or *Luc* KO THP-1 cells were infected with TB40/E-
1169 *UL136*$_{\mathrm{myc}}$ (top panel) or -*UL136*$_{myc}$*ΔK→R* (bottom panel) at a MOI of 2 and cell lysates
1170 were collected at indicated time points. IE1/2 and UL135 accumulation was evaluated
1171 by immunoblotting protein lysates over a time course using a monoclonal α-IE1/2 and
1172 polyclonal α-UL135. (E) IE1, IE2 and UL135 were quantified, and levels normalized to
1173 Tubulin and are shown relative to levels present at 1 dpi in the *Luc* KO control for

1174 *UL136*$_{myc}$ and *UL136*$_{myc}$Δ*K→R* infections. Note that comparisons are made between
1175 *Luc* KO and *IDOL* KO, not between *UL136*$_{myc}$ and *UL136*$_{myc}$Δ*K→R* infections. All data
1176 points are representative as the mean 3 independent replicates and error bars
1177 represent standard deviation. The means were compared by two-way ANOVA with a
1178 Tukey post hoc test. ns, p>0.05; *, p<0.05; **, p<0.01; ****, p<0.0001.
1179
1180 **Figure 6. Induction of IDOL in CD34+ HPCs inhibits reactivation.** (A) CD34+ HPCs
1181 were cultured for 5 days in media with cytokines to stimulate differentiation or left
1182 undifferentiated. RNA was isolated and transcripts encoding IDOL were quantified by RT-qPCR
1183 relative to the H6PD housekeeping gene using the ΔΔCT method. Values were normalized to
1184 the undifferentiated population and graphed for statistical analysis. Statistical significance was
1185 calculated using unpaired student t test and represented by asterisks. Graphs represent the
1186 mean of three replicates and error bars represent SEM. (B) CD34+ HPCs were mock- or
1187 TB40/E-infected at a MOI of 2. At 1 dpi, cells were treated with 1 μM GW3965 for 6 h
1188 and total RNA isolated for qPCR to measure *IDOL* transcript levels relative to *H6PD*.
1189 The data points represent the mean from 3 independent experiments. The means were
1190 analyzed by two-way ANOVA with a Tukey post-hoc test. ***p<0.001; ****, p<0.0001.
1191 (C) CD34+ HPCs were infected at a MOI of 2. At 24 hpi, infected CD34+ cells were
1192 isolated by FACS and seeded into long term culture. GW3965 (1 μM) was added to
1193 induce IDOL at the time of reactivation. At 10 days, half of the culture was reactivated
1194 by seeding intact cells by limiting dilution into co-culture with fibroblasts in a cytokine-
1195 rich media to promote myeloid differentiation (reactivation). The other half of the culture
1196 was mechanically lysed and seeded onto fibroblasts as the pre-reactivation control. The
1197 frequency of infectious centers was determined for each sample by ELDA. The data

1198 points represent replicates from 2 independent donors and the range is indicated by
1199 squares (pre-reactivation) and dots (post-reactivation).

1200

1201 **Figure 7. Model for differentiation-dependent IDOL regulation to control UL136p33**
1202 **levels.** Progenitor cells are relatively small and intolerant of high cholesterol, which they
1203 control, in part, through the expression of IDOL to reduce cholesterol/lipid uptake. We
1204 propose that high levels of IDOL maintain low levels of UL136p33 to restrict HCMV
1205 replication for the establishment of latency following infection. Upon cell differentiation,
1206 the downregulation of IDOL is observed and is expected to correspond to increased
1207 accumulation of UL136p33 to drive reactivation and replication, consistent with our
1208 finding that depletion of IDOL increases HCMV gene expression and that an LXR
1209 agnonist restricts reactivation. We have previously shown that UL136p33 levels further
1210 accumulate in late phase upon the commitment to viral DNA synthesis. Therefore,
1211 following reactivation, we postulate that UL136p33 levels increase due to a combination
1212 of decreased turnover and increased synthesis. Further, because stabilization of
1213 UL136p33 results in corresponding downregulation of IDOL expression, UL136p33 may
1214 feedback to suppress *IDOL* gene expression. This work implicates IDOL as a host
1215 factor that fine-tunes levels of UL136p33 to control decisions to enter and exit latency.
1216 UL136p33 acts as a sensor at the tipping point between the decision to maintain the
1217 latent state or exit latency for reactivation where its instability is critical for the
1218 establishment or latency and its accumulation critical for reactivation. This study
1219 suggests that LXR signaling and cholesterol homeostasis may impact HCMV latency

1220 and reactivation and will be explored in future studies. Figure created with
1221 Biorender.com.
1222
1223
1224

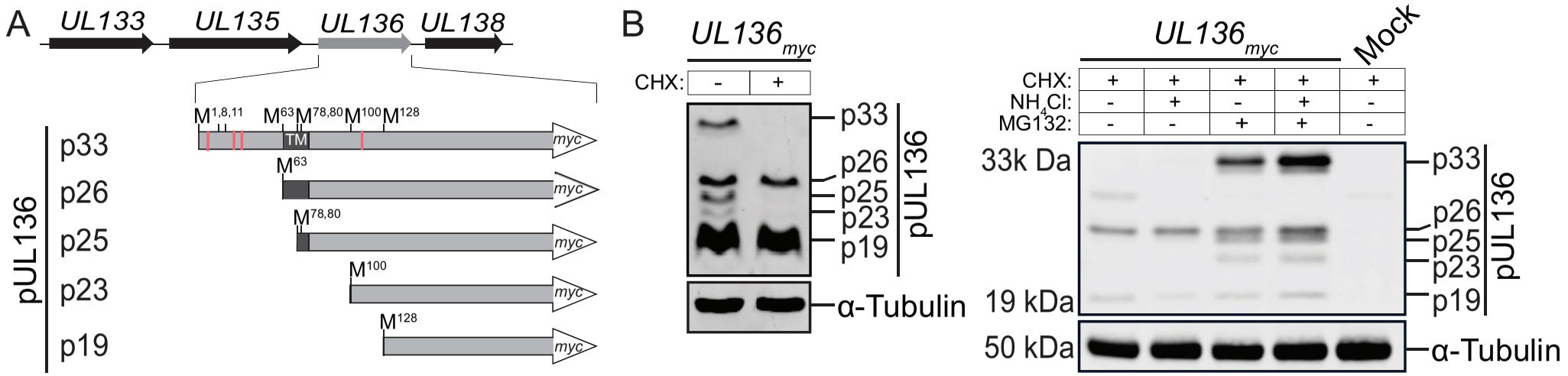
A
UL133
UL135
UL136
UL138
M1,8,11
M63
M78,80
M100
M128
TM
myc
pUL136
p33
p26
p25
p23
p19
B
UL136myc
CHX:
-
+
p33
p26
p25
p23
p19
pUL136
α-Tubulin
UL136myc
Mock
CHX:
NH4Cl:
MG132:
33k Da
19 kDa
50 kDa
α-Tubulin

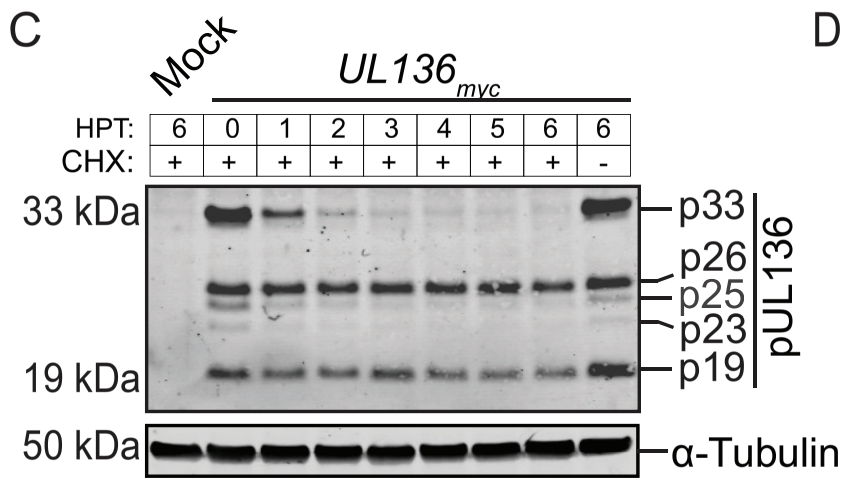
C
Mock
UL136myc
HPT:
CHX:
33 kDa
19 kDa
50 kDa
p33
p26
p25
p23
p19
pUL136
α-Tubulin

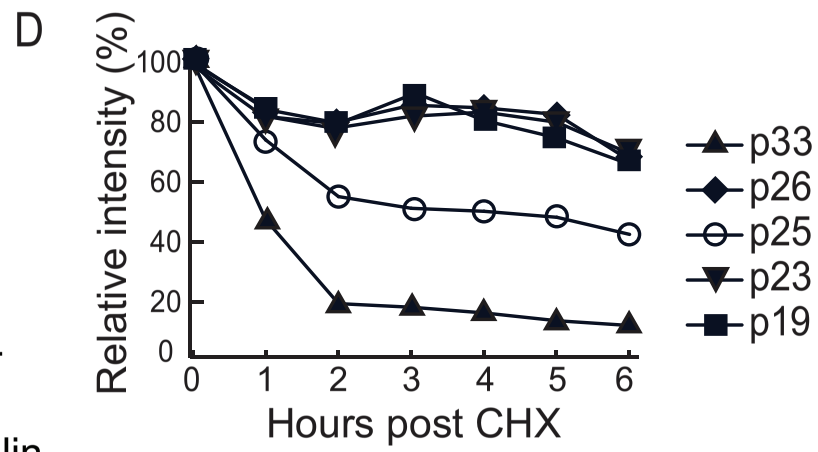
D
Relative intensity (%)
Hours post CHX
p33
p26
p25
p23
p19

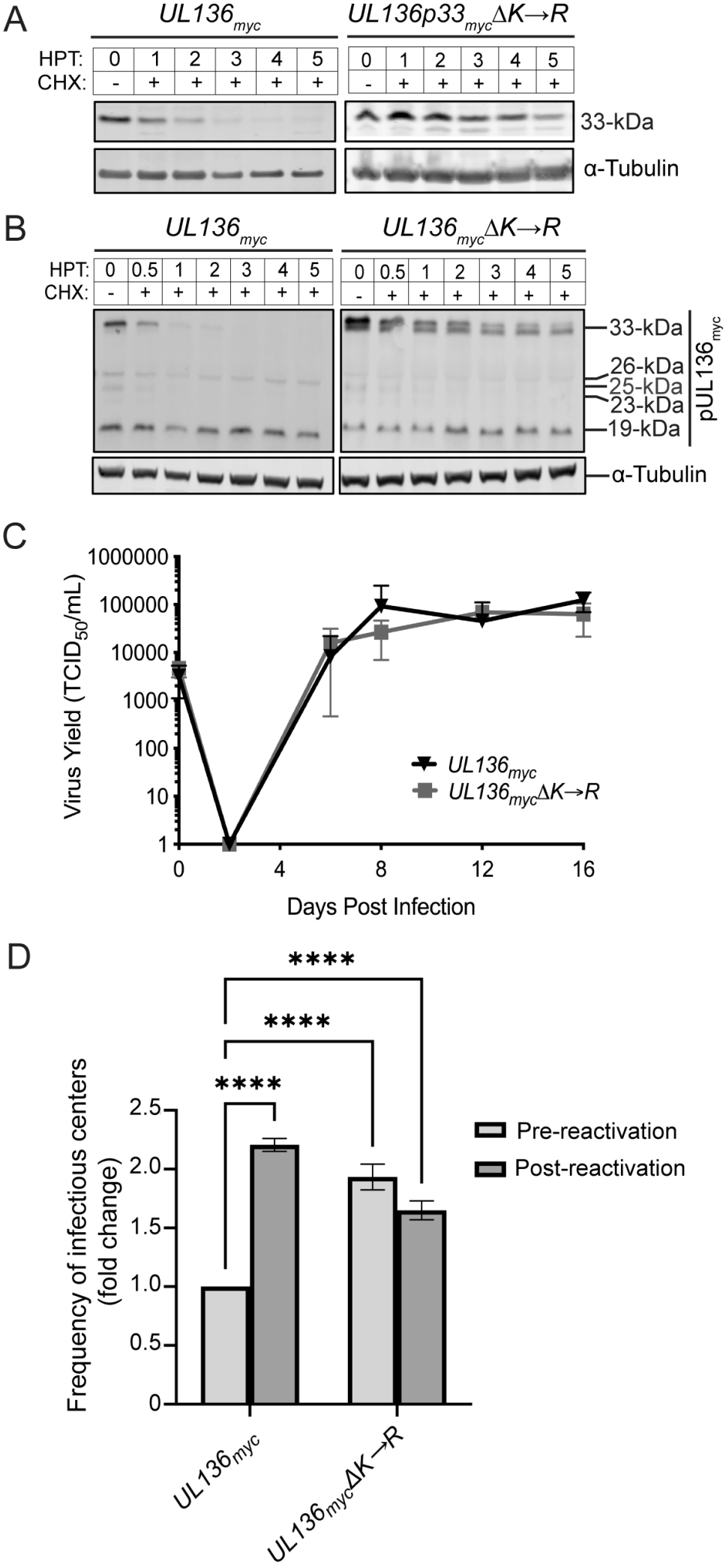
A
UL136myc
UL136p33mycΔK→R
HPT: 0 1 2 3 4 5
CHX: - + + + + +
33-kDa
α-Tubulin
B
UL136myc
UL136mycΔK→R
HPT: 0 0.5 1 2 3 4 5
CHX: - + + + + +
33-kDa
26-kDa
25-kDa
23-kDa
19-kDa
pUL136myc
α-Tubulin
C
Virus Yield (TCID50/mL)
1000000
100000
10000
1000
100
10
1
0
4
8
12
16
Days Post Infection
UL136myc
UL136mycΔK→R
D
Frequency of infectious centers (fold change)
2.5
2.0
1.5
1.0
0.5
0
****
****
****
Pre-reactivation
Post-reactivation
UL136myc
UL136mycΔK→R

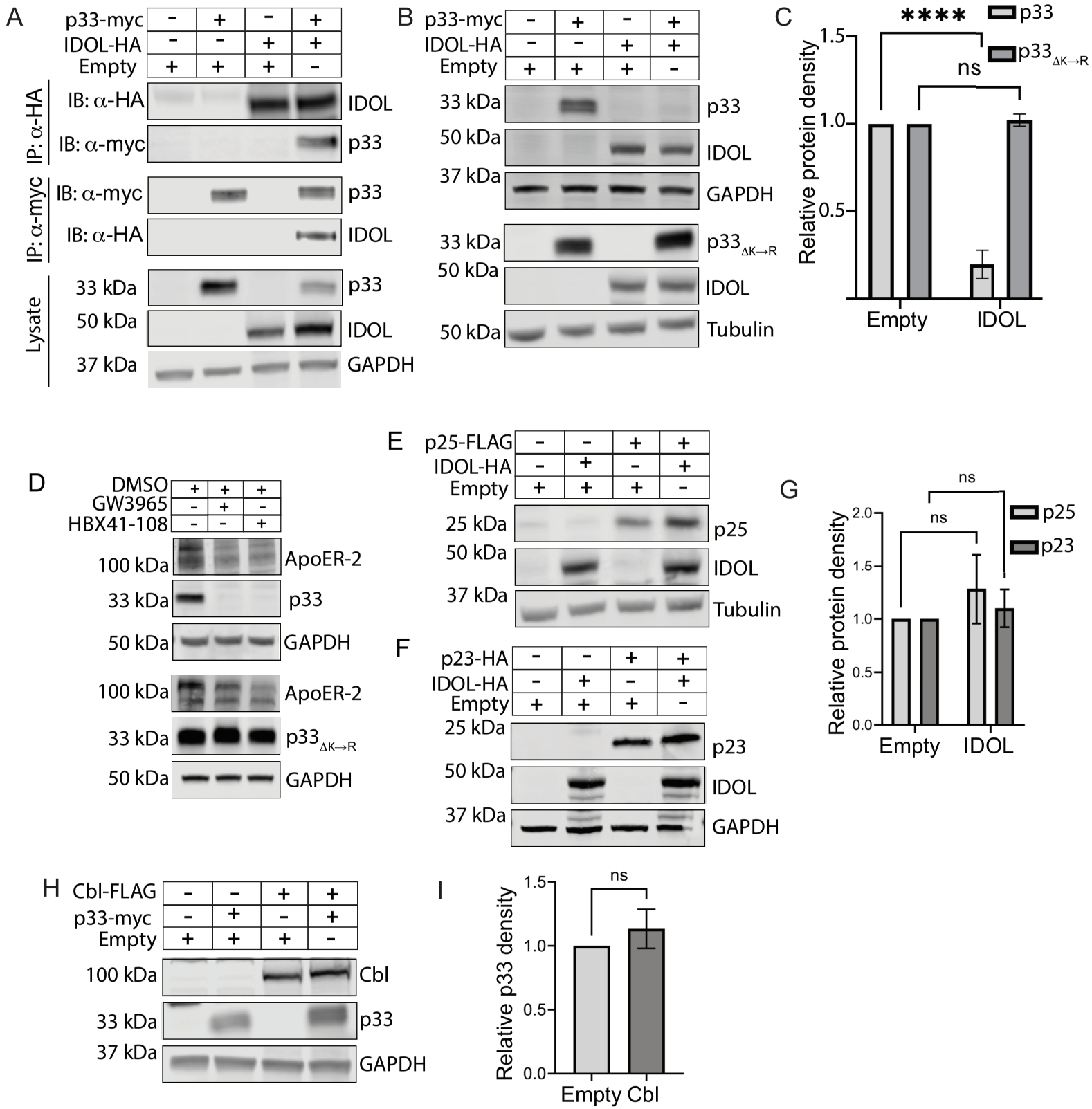
A
p33-myc
IDOL-HA
Empty
IP: α-HA
IB: α-HA
IDOL
IB: α-myc
p33
IP: α-myc
IB: α-myc
p33
IB: α-HA
IDOL
Lysate
33 kDa
p33
50 kDa
IDOL
37 kDa
GAPDH
B
p33-myc
IDOL-HA
Empty
33 kDa
p33
50 kDa
IDOL
37 kDa
GAPDH
33 kDa
p33ΔK→R
50 kDa
IDOL
50 kDa
Tubulin
C
****
ns
p33
p33ΔK→R
Relative protein density
1.5
1.0
0.5
Empty
IDOL
D
DMSO
GW3965
HBX41-108
100 kDa
ApoER-2
33 kDa
p33
50 kDa
GAPDH
100 kDa
ApoER-2
33 kDa
p33ΔK→R
50 kDa
GAPDH
E
p25-FLAG
IDOL-HA
Empty
25 kDa
p25
50 kDa
IDOL
37 kDa
Tubulin
F
p23-HA
IDOL-HA
Empty
25 kDa
p23
50 kDa
IDOL
37 kDa
GAPDH
G
ns
ns
p25
p23
Relative protein density
2.0
1.5
1.0
0.5
0.0
Empty
IDOL
H
Cbl-FLAG
p33-myc
Empty
100 kDa
Cbl
33 kDa
p33
37 kDa
GAPDH
I
ns
Relative p33 density
1.5
1.0
0.5
0.0
Empty
Cbl

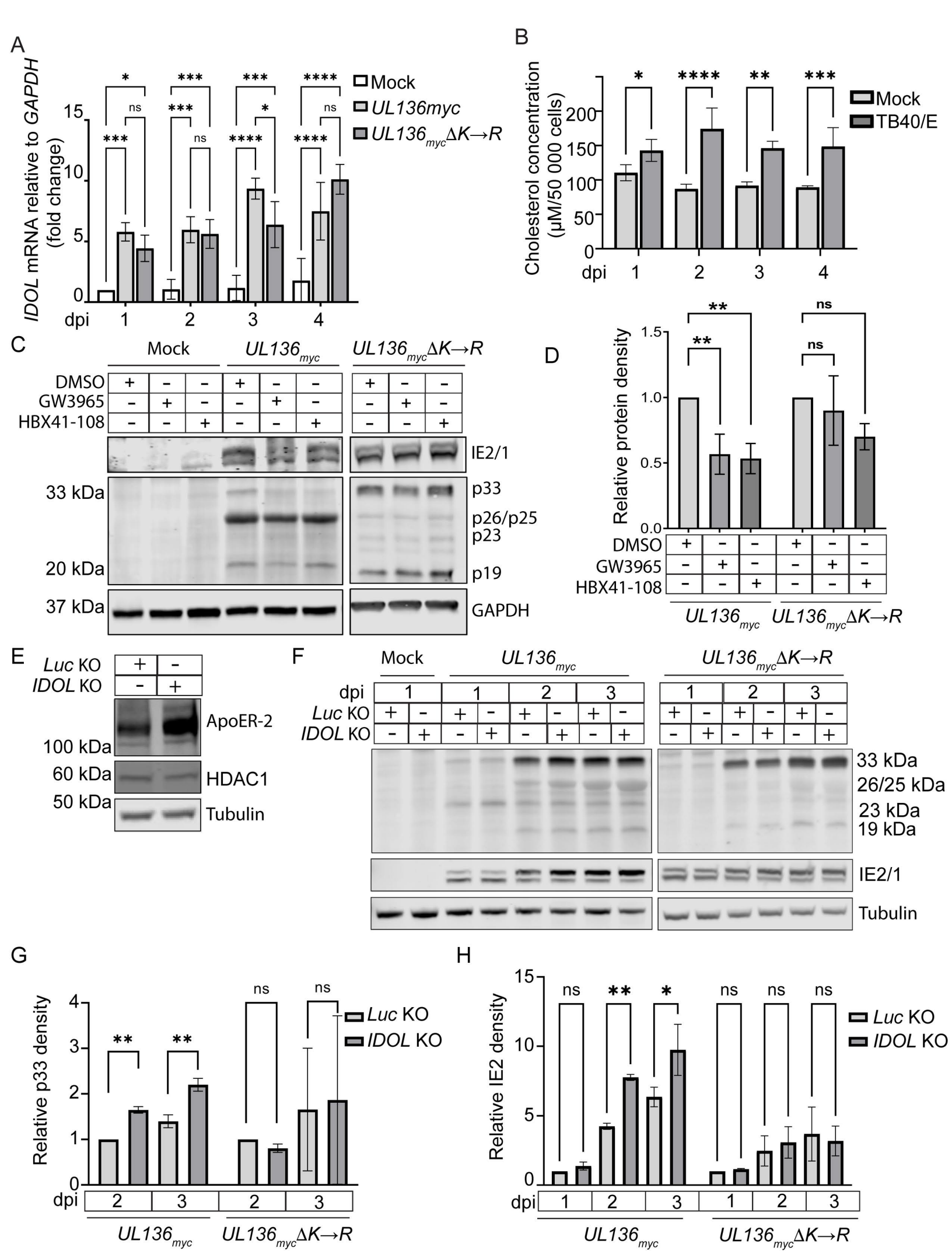
A
IDOL mRNA relative to GAPDH (fold change)
Mock
UL136myc
UL136mycΔK→R
dpi
B
Cholesterol concentration (µM/50 000 cells)
Mock
TB40/E
C
Mock
UL136myc
UL136mycΔK→R
DMSO
GW3965
HBX41-108
IE2/1
33 kDa
20 kDa
37 kDa
p33
p26/p25
p23
p19
GAPDH
D
Relative protein density
E
Luc KO
IDOL KO
ApoER-2
100 kDa
60 kDa
50 kDa
HDAC1
Tubulin
F
dpi
33 kDa
26/25 kDa
23 kDa
19 kDa
IE2/1
Tubulin
G
Relative p33 density
Luc KO
IDOL KO
H
Relative IE2 density

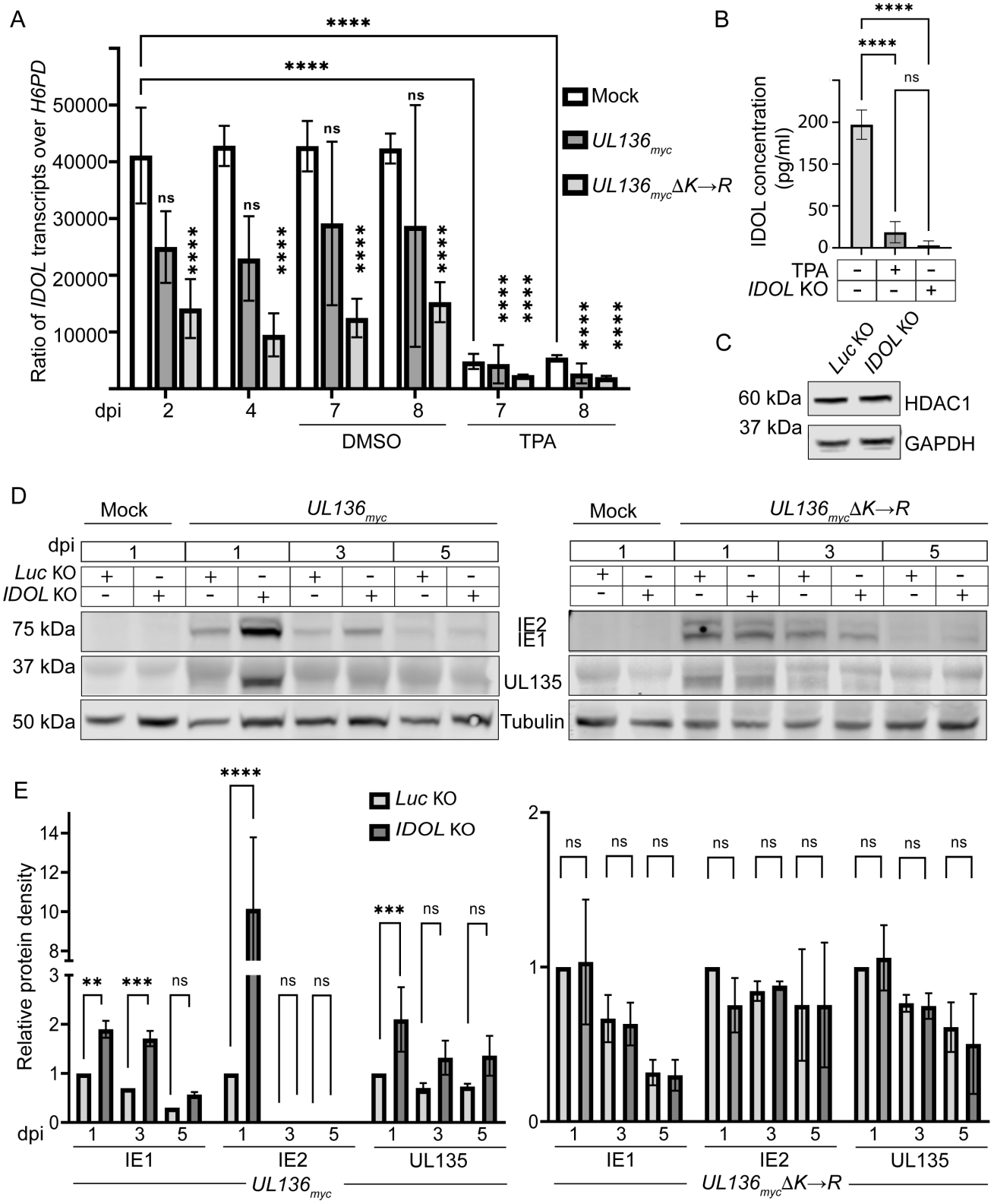
A
Ratio of IDOL transcripts over H6PD
50000
40000
30000
20000
10000
****
****
ns
ns
ns
ns
Mock
UL136myc
UL136mycΔK→R
dpi
2
4
7
8
7
8
DMSO
TPA
B
IDOL concentration (pg/ml)
200
150
50
0
****
****
ns
TPA
IDOL KO
C
Luc KO
IDOL KO
60 kDa
HDAC1
37 kDa
GAPDH
D
Mock
UL136myc
Mock
UL136mycΔK→R
dpi
1
1
3
5
Luc KO
IDOL KO
75 kDa
37 kDa
50 kDa
IE2
IE1
UL135
Tubulin
E
Relative protein density
Luc KO
IDOL KO
**
***
ns
****
ns
ns
***
ns
ns
dpi
IE1
IE2
UL135
UL136myc
UL136mycΔK→R

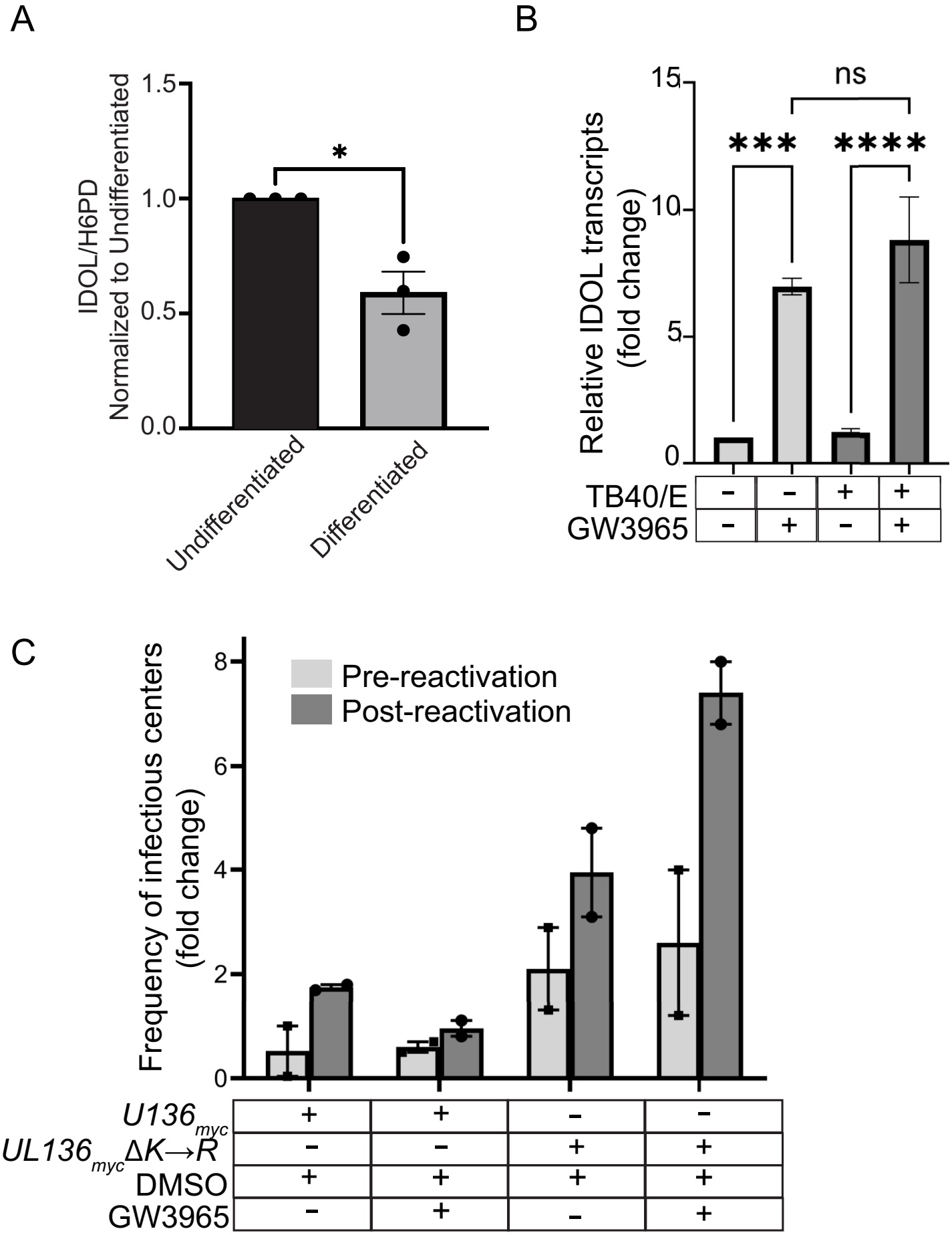
A
IDOL/H6PD
Normalized to Undifferentiated
1.5
1.0
0.5
0.0
*
Undifferentiated
Differentiated
B
Relative IDOL transcripts
(fold change)
15
10
5
0
ns
***
****
TB40/E
GW3965
C
Frequency of infectious centers
(fold change)
8
6
4
2
0
Pre-reactivation
Post-reactivation
U136myc
UL136myc ΔK→R
DMSO
GW3965

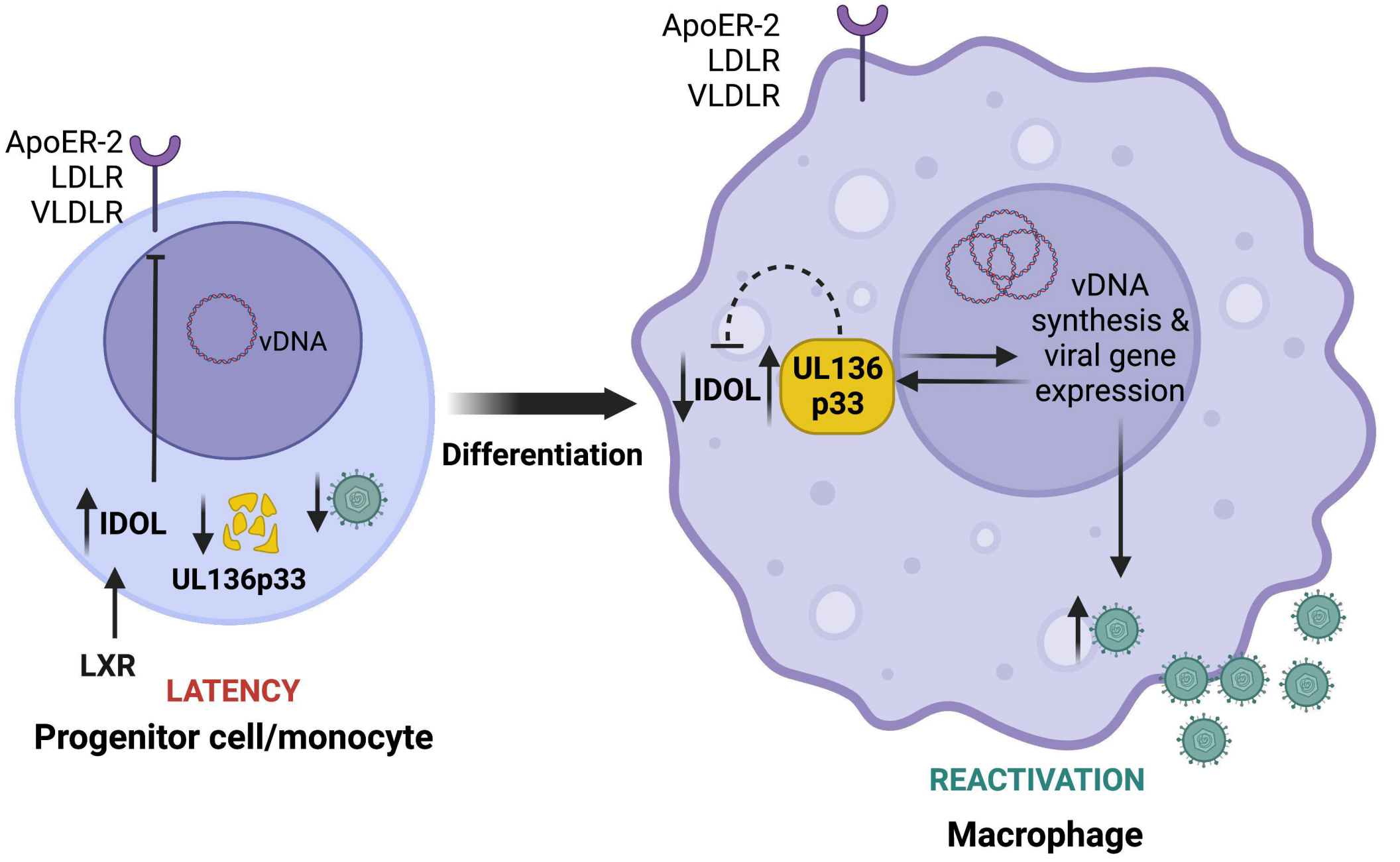
ApoER-2
LDLR
VLDLR
vDNA
IDOL
UL136p33
LXR
LATENCY
Progenitor cell/monocyte
Differentiation
ApoER-2
LDLR
VLDLR
IDOL
UL136
p33
vDNA
synthesis &
viral gene
expression
REACTIVATION
Macrophage